Geological Society of America Bulletin

Coupled U-Pb dating and Hf isotopic analysis of detrital zircon of modern river sand from the Yalu River (Yarlung Tsangpo) drainage system in southern Tibet: Constraints on the transport processes and evolution of Himalayan rivers

J.Y. Zhang, A. Yin, W.C. Liu, F.Y. Wu, Ding Lin and M. Grove

Email alerting services	click www.gsapubs.org/cgi/alerts to receive free e-mail alerts when new articles cite this article
Subscribe	click www.gsapubs.org/subscriptions/ to subscribe to Geological Society of America Bulletin
Permission request	click http://www.geosociety.org/pubs/copyrt.htm#gsa to contact GSA

Notes

THE
GEOLOGICAL
SOCIETY
OF AMERICA

Coupled U-Pb dating and Hf isotopic analysis of detrital zircon of modern river sand from the Yalu River (Yarlung Tsangpo) drainage system in southern Tibet: Constraints on the transport processes and evolution of Himalayan rivers

J.Y. Zhang[1,†], A. Yin[1,2,†], W.C. Liu[1,†], F.Y. Wu[3,†], Ding Lin[4,†], and M. Grove[5,†]

[1]*Structural Geology Group, China University of Geosciences (Beijing), Beijing 100083, China*
[2]*Department of Earth and Space Sciences, University of California, Los Angeles, California 90095-1567, USA*
[3]*State Key Laboratory of Lithospheric Evolution, Institute of Geology and Geophysics, Chinese Academy of Sciences, P.O. Box 9825, Beijing 100029, China*
[4]*Institute of Tibetan Plateau Research, Chinese Academy of Sciences, P.O. Box 9825, Beijing 100085, China*
[5]*Department of Geological & Environmental Sciences, Stanford University, Stanford, California 94305, USA*

ABSTRACT

We conducted coupled U-Pb dating and Hf isotope analysis of detrital zircon in modern sand of the Yalu River in southern Tibet. Our work indicates that the presence or absence of distinctive zircon populations in the Yalu main stream depends critically on the geometric configuration of the tributary rivers. The proportion of upper-stream zircon populations in the Yalu River sand decreases systematically in the downstream direction, which is caused mainly by zircon addition from new source areas in the downstream region. In some extreme cases, the upstream zircon signals can completely be lost in the downstream region due to this dilution effect. Analysis of sand modal composition reveals a downstream increase in the proportion of lithic fragments along the Yalu River, from ~40% to ~60% over a distance of ~600 km. This may be attributed to the combined effect of an eastward increase in the topographic relief and an eastward increase in annual precipitation across the Yalu River drainage basin. Quantitative comparison of detrital-zircon ages between the Yalu River sand and Neogene sediments of the eastern Himalayan foreland supports a previous proposal that the Yalu River once flowed directly over the eastern Himalaya, without going around the Himalaya through its eastern syntaxis. The shortcut appears to have been transient, as it is only recorded in specific stratigraphic horizons of foreland sediments. The inferred Yalu River diversion may have been caused by past advances of glaciers or emplacements of giant landslides that temporarily dammed the Yalu River.

INTRODUCTION

The evolution of major river systems in the Indo-Asian collision zone is closely related to lithospheric deformation, climate change, and temporal variation of biodiversity (e.g., Seeber and Gornitz, 1983; Brookfield, 1998; Zeitler et al., 2001; Hallet and Molnar, 2001; Clark et al., 2004, 2006; Thiede et al., 2005; Montgomery and Stolar, 2006; Clift, 2006, 2008a, 2008b; Grujic et al., 2006; Finnegan et al., 2008; Robl et al., 2008; Che et al., 2010; Hoorn et al., 2010). In recent years, U-Pb dating of detrital zircon has been widely used in reconstructing Himalayan deformation, exhumation history, sedimentation processes, and drainage evolution (e.g., DeCelles et al., 2000, 2004; Gehrels et al., 2003; Iizuka et al., 2005; Amidon et al., 2005; Liang et al., 2008; McQuarrie et al., 2008; Stewart et al., 2008; Cina et al., 2009; Myrow et al., 2009; Yin et al., 2006, 2010a, 2010b; Wu et al., 2007, 2010; Tobgay et al., 2010; Enkelmann et al., 2011; Webb et al., 2011; Gehrels et al., 2011). However, the linkage between zircon populations in the source regions and those in the sinks (i.e., foreland basin) in the active Himalayan orogen has not been systematically explored by any previous work.

The main goal of this paper is to use coupled U-Pb dating and Hf isotope analysis of detrital zircon to determine zircon-population distributions in the Yalu River and its tributaries. The approach allows characterization of zircon populations along different segments of the Yalu River and its tributaries. Comparison of zircon populations in the Yalu drainage system and those of bedrock allows us to quantify the spatial relationships of zircon populations in the two systems and the processes that transfer zircon populations from the source regions to the foreland basin. In addition, comparisons of zircon populations along different segments of the Yalu River and its tributaries against those of the late Cenozoic (younger than 10 Ma) deposits in the Himalayan foreland provide clues for possible geometry of fluvial delivery systems in the recent past that linked the most likely source areas with the terminus of sedimentation in the foreland.

REGIONAL GEOLOGY AND BEDROCK AGES

The Yalu River, linking the Brahmaputra River via the Siang River and merging with the Ganges River, flows into the Bay of Bengal (Fig. 1A). The total length of the drainage system exceeds 2500 km. Although the river follows broadly along the Indus-Tsangpo suture, the course departs locally to the north and south (Fig. 1B).

The Lhasa terrane (Fig. 1B), located north of the Indus-Tsangpo suture, consists of metavolcanic and orthogneiss units that yield U-Pb zircon ages of 501 ± 2 Ma, 531 ± 14 Ma, 748 ± 8 Ma, 787 ± 9 Ma, and 852 ± 18 Ma (Xu et al., 1985; Hu et al., 2005; Guynn et al., 2006; Ji et al., 2009). They are overlain by Ordovician

†E-mails: jinyuzhang86@gmail.com; yin@ess.ucla.edu; liuwenc@263.net; wufuyuan@mail.iggcas.ac.cn; dinglin@itpcas.ac.cn; mjgrove@stanford.edu

to Permian marine strata, Triassic siliciclastic and volcaniclastic rocks, Jurassic turbidites and volcanic flows, and Cretaceous shallow-marine strata and volcanic and sedimentary rocks, which are widely exposed in the Lhasa terrane (Leeder et al., 1988; Yin et al., 1994; Murphy et al., 1997; Yin and Harrison, 2000; Pan et al., 2004; Kapp et al., 2005, 2007a; Wu et al., 2010). The Late Jurassic to Early Tertiary Gangdese igneous belt, located in the southern and central Lhasa terrane (Yin and Harrison, 2000) (Fig. 1B), can be divided into the northern and southern zones based on age and isotopic composition. The southern zone is dominated by ca. 50 Ma I-type granitoids with positive $\varepsilon_{Hf}(t)$ values (Harrison et al., 2000; Kapp et al., 2005; Chu et al., 2006; Mo et al., 2007; Wen et al., 2008; Ji et al., 2009; Ji, 2010; Wu et al., 2010; Zhu et al., 2011), whereas the northern zone is composed mostly of 110–115 Ma S-type granitoids with negative $\varepsilon_{Hf}(t)$ values (Xu et al., 1985; Harris et al., 1990; Chu et al., 2006; Chiu et al., 2009). Scattered volcanic rocks, dikes, and small plutons with zircon ages of 30–10 Ma and positive $\varepsilon_{Hf}(t)$ values also occur across the Lhasa terrane (Yin et al., 1994; Miller et al., 1999; Williams et al., 2001; Sun et al., 2008; Chung et al., 2009). Leucogranites with ages of 25–20 Ma exist in the southwestern Lhasa terrane (e.g., Lacassin et al., 2004).

The Himalayan orogen south of the Indus-Tsangpo suture consists of, from the highest to lowest structural levels, the Tethyan Himalayan Sequence, the Greater Himalayan Crystalline Complex, and the Lesser Himalayan Sequence (Gansser, 1964; LeFort, 1975; Burchfiel et al., 1992; Yin and Harrison, 2000; Yin, 2006) (Fig. 1B). The Tethyan Himalayan Sequence unit displays detrital-zircon age clusters at 500 Ma and 1100 Ma (Gehrels et al., 2003; Myrow et al., 2003, 2009, 2010; DeCelles et al., 2000, 2004; Yin et al., 2006, 2010a, 2010b; McQuarrie et al., 2008; Tobgay et al., 2010). It also consists of Triassic basalts (see review in Yin, 2006), Early Cretaceous volcanic rocks (LeFort and Räi, 1999; Zhu et al., 2005, 2007, 2008a, 2008b, 2009a; Hu et al., 2010), and Eocene to Miocene granites (e.g., Harrison et al., 1998; Aikman et al., 2008; Zeng et al., 2011). The Tethyan Himalayan Sequence unit in the eastern Himalaya displays a zircon population with ages ranging from 220 Ma to 265 Ma (Aikman et al., 2008). The Greater Himalayan Crystalline Complex unit is dominated by age clusters of detrital zircon at 1100, 1500–1700, and 2500–2600 Ma (Gehrels et al., 2003, 2011; DeCelles et al., 2004). The Greater Himalayan Crystalline Complex also contains 500 Ma, 825–870 Ma, and ca. 1.7 Ga orthogneiss in the eastern Himalaya (DeCelles et al., 2000; Gehrels et al., 2003;
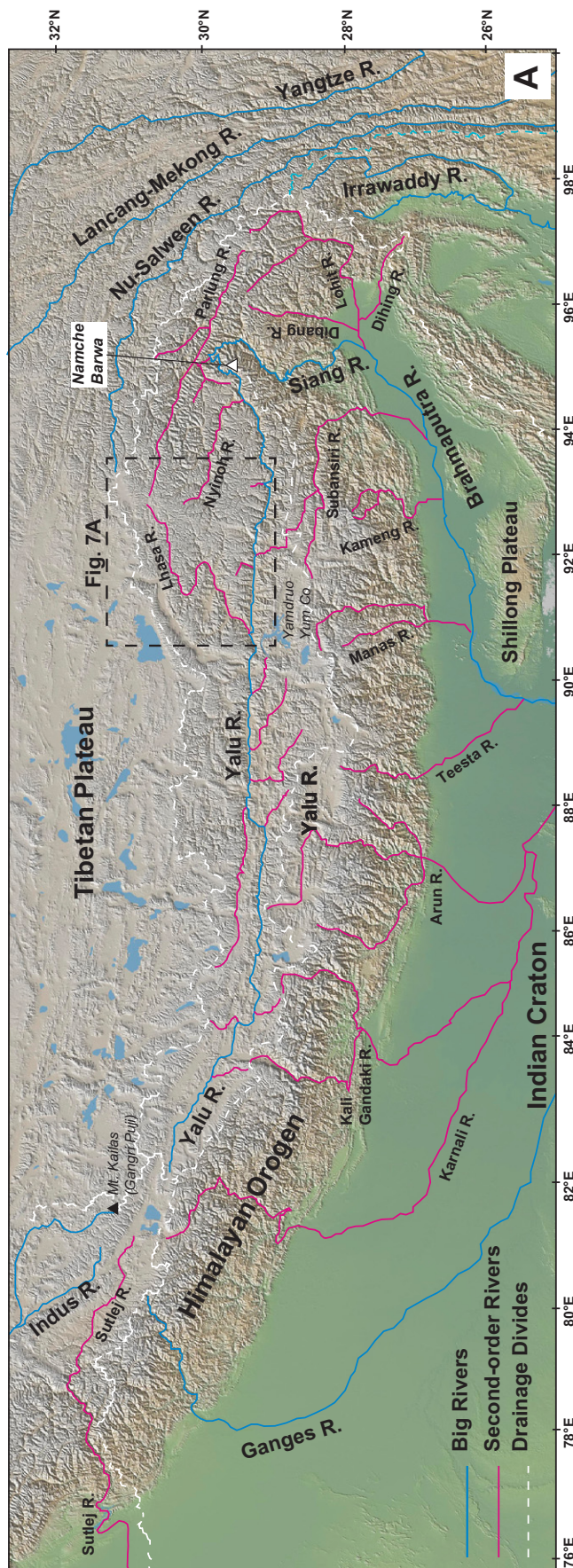
Figure 1 (*on this and following two pages*). (A) The digital topographic map of the southern Tibetan Plateau and the Himalayan orogen based on the Global Multi-Resolution Topography (GMRT) Synthesis by Ryan et al. (2009) (http://www.geomapapp.org). The main streams of the Yalu River, Siang River, and Brahmaputra River are marked by blue lines; their tributaries are marked by purple lines. Major drainage divides are outlined by dotted lines.

Coupled U-Pb dating and Hf isotopic analysis of detrital zircon of modern river sands from the Yalu River
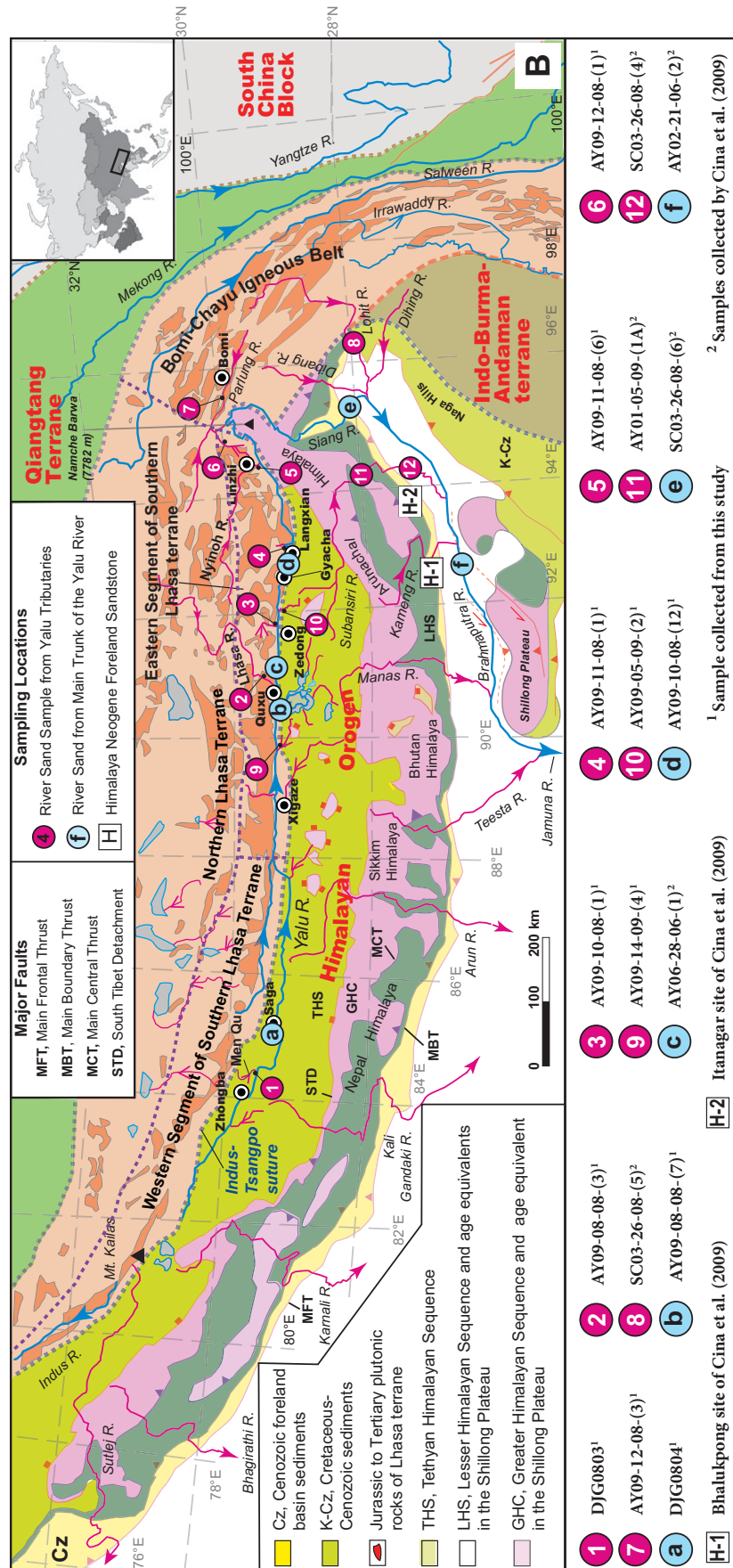
Figure 1 (*continued*). (B) Regional tectonic map with simplified geology of the Lhasa terrane and the Himalayan orogen. Also shown are major rivers and sampling sites (also see Table 1). Numbers 1 to 12 mark locations of modern sand samples from tributaries of the Yalu River, whereas letters a to f represent sample locations of modern sand samples from the main trunk of the Yalu River. Samples from sites 8, 11, 12, c, e, and f were collected and analyzed by Cina et al. (2009), while the rest of the samples were collected in this study. Sites H-1 and H-2 represent sample sites of Neogene sandstone from Himalayan foreland basin by Cina et al. (2009). H-1 represents the Bhalukpong site of Cina et al. (2009), and H-2 represents the Itanagar site of Cina et al. (2009).

Zhang et al.
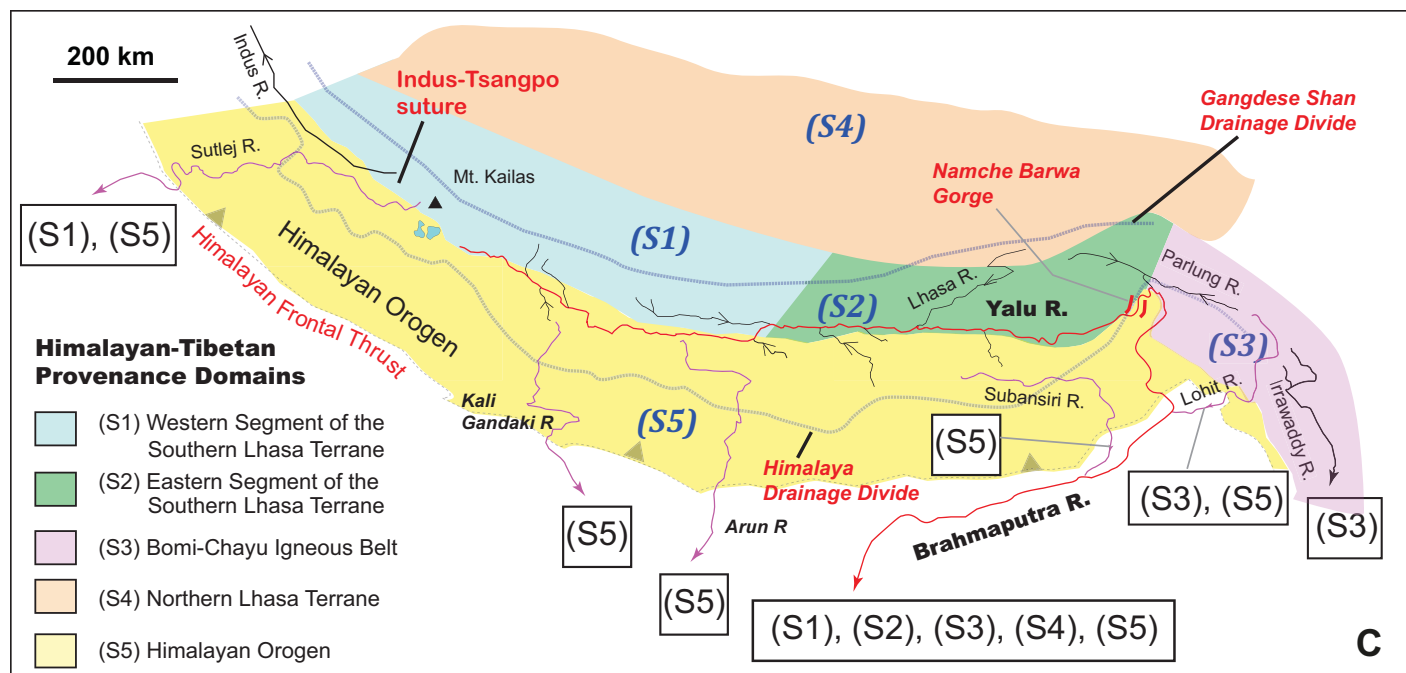
Figure 1 (*continued*). (C) Division of provenance domains in the Yalu River drainage basin: S1 represents the western segment of the southern zone of the Lhasa belt; S2 represents the eastern segment of the southern zone of the Lhasa terrane; S3 represents the north-trending Bomi-Chayu igneous belt east of the eastern Himalayan syntaxis; S4 represents the northern zone of the Lhasa terrane; and S5 represents the Himalayan orogen.

Yin et al., 2010b). Miocene leucogranites intrude extensively across the unit (e.g., LeFort and Räi, 1999; Harrison et al., 1998). The Lesser Himalayan Sequence, including orthogneiss dated between 2.1 Ga and 1.7 Ga, displays age peaks of detrital zircons at 470–490 Ma, 1.1 Ga, 1.65–1.85 Ga, and 2.5 Ga (DeCelles et al., 2000, 2004; Yin et al., 2010b).

Five provenance domains in the Yalu River basin are shown in Figure 1C. Each domain is defined by U-Pb zircon ages using relative probability plots (Figs. 2A–2E and 2I) and $\varepsilon_{Hf}(t)$ isotope values (Figs. 2F–2H and 2J) (data sources of each domain can be found in Supplemental Item A in the GSA Data Repository[1]). Although the age spectra of bedrock are compared to those of detrital zircon from river sand in this study, we are aware of the limitations, such as nonsystematic sampling of bedrock biased toward easily accessed areas, differential rates of sediment production controlled by lithology, relief, precipitation, surface processes, time-dependent erosion, and burial of source rocks, and differential discharge between water and sediments in rivers. Despite these complications, the first-

order age peaks are highly diagnostic. For example, both the age spectra of bedrock and detrital zircon from river sand are distinctively different. In addition, bedrock zircon ages and the corresponding Hf values are diagnostic for differentiating source domains such as the northern and southern zones of the Gangdese igneous belt (see detailed description in Supplemental Item A in the GSA Data Repository [see footnote 1]).

Studies of ages, cooling histories, and composition of Yalu River sand around the eastern

Himalayan syntaxis suggest that this region contributes >50% of the current sediment load in the downstream Brahmaputra River (e.g., Garzanti et al., 2004; Stewart et al., 2008; Enkelmann et al., 2011). Based on the correlation of age spectra of detrital zircon from the Yalu, Siang, and Brahmaputra Rivers, Cina et al. (2009) speculated that the Yalu River may have once flowed directly across the eastern Himalaya without going around the eastern Himalayan syntaxis. Although these studies provide important con-

[1]GSA Data Repository item 2012210, U-Pb zircon ages and Hf isotope values of bedrock, and river sand, is available at http://www.geosociety.org/pubs/ft2012.htm or by request to editing@geosociety.org.

Figure 2 (*on following page*). Relative probability plots of bedrock zircon U-Pb ages (Ma) at the range of 0–300 Ma from the Himalayan orogen (Him.) and the Lhasa terrane (LT): **(A)** the northern Lhasa terrane (NL), **(B)** the western segment of the southern Lhasa terrane (WL), **(C)** the eastern segment of the southern Lhasa terrane (EL), **(D)** the Bomi-Chayu igneous belt (BCh), and **(E)** Himalayan orogen (Him.), and **(F–H)** the corresponding plots of U-Pb ages versus $\varepsilon_{Hf}(t)$ values, **(I)** a combined relative probability diagram for U-Pb ages from the Himalayan orogen (Him.) and Lhasa terrane (LT) (note different scales for the ages from the Himalayan orogen and Lhasa terrane), and **(J)** a display of the U-Pb age spectra versus the $\varepsilon_{Hf}(t)$ values for bedrock zircon from the Himalayan orogen and Lhasa terrane with ages older than 300 Ma. Quoted data for the Lhasa terrane are shown in Supplemental Item A in the GSA Data Repository (see text footnote 1) as well as $^{40}Ar/^{39}Ar$ ages from Lee et al. (2009, and references therein), while those for the Himalayan orogen are from DeCelles et al. (2004), Gehrels et al. (2003), McQuarrie et al. (2008), Myrow et al. (2009, 2010), Tobgay et al. (2010), Hu et al. (2010), Li et al. (2010), Zhu et al. (2005, 2007, 2008a, 2008b, 2009a), Aikman et al. (2008), Zeng et al. (2011), and King et al. (2011), and references therein. THS—Tethyan Himalayan Sequence.

Coupled U-Pb dating and Hf isotopic analysis of detrital zircon of modern river sands from the Yalu River

Figure 2.

Zhang et al.

straints on the evolution of the Yalu River around the Namche Barwa region, the sampling coverage is less than 2% of the total area for the Yalu-Siang-Brahmaputra drainage system. For example, there was only one sample collected by Cina et al. (2009) from the main trunk of the Yalu River west of longitude 91.1°E, beyond which the river flows for another 1000 km. Also, note that none of the above studies made any effort to systematically document age distribution of bedrock across the entire Yalu River watersheds, which is accomplished for the first time in this study. Finally, this study reports for the first time age spectra of detrital zircon from tributaries of the Yalu River west of longitude 91°E draining across both the Lhasa terrane and the Himalayan orogen. Together, the newly compiled and obtained age data allow a systematic investigation of zircon age variations from source regions, through tributaries, and finally to the main trunk of the Yalu River and the Himalayan foreland basin.

SAMPLE COLLECTION AND ANALYTICAL METHODS

In total, 12 river sand samples were collected from (1) the Yalu River, (2) short Yalu tributaries across the southern Gangdese igneous belt, (3) long Yalu tributaries across the entire Gangdese igneous belt, and (4) Himalayan tributaries of the Yalu River (Fig. 1B). Sample collection was conducted in August and September at the end of or immediately after the Indian summer monsoon season. This time period was selected because high precipitation and thus high discharge should have caused the most intense erosion and thus maximum delivery of bedrock zircon populations into the Yalu drainage system.

All samples were collected from medium-grained sand, with each sample weighing ~5 kg. We tried to collect samples from braided bars in the central courses of river channels wherever possible. Where no braided bars were exposed, we collected samples from point bars at the edges closest to the flowing rivers to avoid contamination of sand from potentially locally derived bank materials. We also chose our sample sites away from any landslides common at narrow gorges of the Yalu River (i.e., Finnegan et al., 2008). Finally, we avoided sampling sites from tributary confluences to avoid bias toward one particular source.

Once collected, the sand samples were sent to the Institute of Hebei Regional Geology and Mineral Survey in Langfang, Hebei Province, for mineral separation. The dried river sand was first crushed to pass a 60 mesh (250 μm) sieve. Manual washing with water and then alcohol was performed carefully for multiple aliquots

of the crushed material to get the denser component of various grain sizes. An electromagnetometer was then used to remove magnetic minerals. Heavy liquid separation was used to concentrate heavy minerals, and the remaining non-zircon minerals were picked out by hand under a binocular, leaving only zircon grains in the sample. The zircon grains were mounted randomly in epoxy resin and polished close to one-third of individual grain diameters. It is believed that at least 59 randomly selected grains should be measured to reduce the probability of missing one population comprising >5% of the total at a 95% significance level (Dodson et al., 1988). In this study, we aimed at analyzing at least 75 grains from each sample.

Simultaneous analyses of U-Pb and Hf isotopic compositions of detrital-zircon grains from 10 samples (i.e., samples from sites 1–7 and sites a, b, and d in Fig. 1B) were carried out at the Institute of Geology and Geophysics, Chinese Academy of Sciences, using an Agilent 7500a multicollector–inductively coupled plasma–mass spectrometer (MC-ICP-MS) and a Neptune MC-ICP-MS equipped with a 193 nm excimer ArF laser-ablation system. Each analysis was composed of an ~30 s background measurement with laser off and a 60 s measurement of peak intensities. The ablation pits varied at 40, 50, and 60 μm in diameter, which depended on the size of sample grains, and at ~30–40 μm in depth. The ablated material was carried in helium into the Q-ICP-MS and MC-ICP-MS for simultaneous determination of U-Pb age and Hf isotopic values. The analytical method used in this study follows Xie et al. (2008). Standard zircon 91500 was employed to correct for mass bias affecting $^{207}Pb/^{206}Pb$, $^{206}Pb/^{238}U$, $^{207}Pb/^{235}U$ ($^{235}U = {}^{238}U/137.88$), and $^{208}Pb/^{232}Th$ ratios. NIST SRM 610 glass was used for concentration information and the U/Th ratio determination. The fractionation correction and results were calculated using GLITTER 4.0 (Macquarie University), and common Pb was corrected following the method described by Andersen (2002). The analytical data for U-Pb zircon dating are shown in Supplemental Item B in the GSA Data Repository, while the corresponding data for Hf isotope analysis are shown in Supplemental Item C in the GSA Data Repository (see footnote 1). The interpreted U/Pb ages are based on $^{206}Pb*/^{238}U$ for grains younger than 1000 Ma and $^{207}Pb*/^{206}Pb*$ for grains older than 1000 Ma, with uncertainties both at the 1σ level. Considering potential signal instability resulting from simultaneous measurements of U-Pb and Lu-Hf isotope systems, we generally filtered our results to include analyses that had <30% discordance or <10% reverse discordance. For Lu-Hf isotopic analysis, we ignored the inter-

ference of ^{176}Lu on ^{176}Hf due to normally low $^{176}Lu/^{177}Hf$ ratios in zircon (<0.002), and ^{176}Yb interference corrections were performed using average β_{Yb} values assuming $^{176}Yb/^{172}Yb = 0.5887$, following Wu et al. (2006). Cathodoluminescence (CL) imaging was employed to investigate the rim-core relationships. For grains with cores and rims, we analyzed only the rims, as their ages record the most recent thermal events.

The U-Pb dating of detrital zircon from two samples (i.e., samples from sites 9 and 10 in Fig. 1B) was conducted using an Agilent 7500a Q-ICP-MS with a 193 nm excimer ArF laser-ablation system at the Institute of Tibetan Plateau Research, Chinese Academy of Science. The first 15 s with the laser-off mode were used to collect the background values, and the following 40 s with the laser-on mode were employed to measure the peak intensities of the ablated material. Considering the size distribution of these detrital-zircon grains and signal stability, we adapted 25 μm ablation pits for all grains. The analytical procedure is similar to Xie et al. (2008) using Plesovice zircon and NIST SRM 612 as standards.

Modal compositions of sand samples were analyzed using the following procedure. Sand grains were mounted with epoxy resin on thin sections, and at least 300 grains were counted using the Gazzi-Dickinson method (Gazzi, 1966; Dickinson, 1970; Ingersoll et al., 1984; Dickinson, 1985). The grain types were identified and tabulated following Ingersoll et al. (1984) and Dickinson (1985). As our intention was to determine the first-order trend, we only tabulated quartz (Q), feldspar (F), and lithic fragments (L) in our analysis. K-feldspar and plagioclase were differentiated optically.

RESULTS OF U-Pb DETRITAL-ZIRCON DATING

The following description includes 12 river sand samples collected in this study (Table 1). Results of five samples from our previous work by Cina et al. (2009) are also summarized here for comparison.

Short Tributaries in the Lhasa Terrane

Men Qu

Sample DJG0803 (site 1 in Fig. 1B) was collected from the south-flowing Men Qu (Qu = river in Tibetan) directly east of Zhongba (~84.6°E). Although the river is located north of the Yalu River, its catchment covers mostly the Himalayan orogen as the Yalu River lies south of the suture in this area (Fig. 1B). U-Pb dating indicates that ~70% zircon is younger than

TABLE 1. SUMMARY OF SAMPLE NUMBERS AND SAMPLE LOCATIONS

Sample number	Description	Type	Latitude (°N)	Longitude (°E)	Location in detail	Data source
Short tributaries in the Lhasa terrane						
DJG0803	River sand	Tributary	29.5434	84.6179	Men Qu, site 1 in Fig. 1B	This study
AY09-10-08-(1)	River sand	Tributary	29.2837	91.8158	Zedong, site 3 in Fig. 1B	This study
AY09-11-08-(1)	River sand	Tributary	29.1410	93.1350	Langxian, site 4 in Fig. 1B	This study
AY09-12-08-(1)	River sand	Tributary	29.9888	94.8750	Layue Qu, site 6 in Fig. 1B	This study
Long tributaries in the Lhasa terrane						
AY09-08-08-(3)	River sand	Tributary	29.4426	90.9315	Lhasa River, site 2 in Fig. 1B	This study
AY09-11-08-(6)	River sand	Tributary	29.4333	94.4543	Nyingoh River, site 5 in Fig. 1B	This study
AY09-12-08-(3)	River sand	Tributary	29.9084	95.4606	Parlung River, site 7 in Fig. 1B	This study
SC03-26-08-(5)	River sand	Tributary	27.8781	96.3600	Lohit River, site 8 in Fig. 1B	Cina et al. (2009)
Yalu and Brahmaputra tributaries across the Himalayan orogen						
AY09-14-09-(4)	River sand	Tributary	29.2959	89.7952	Renbu Qu, site 9 in Fig. 1B	This study
AY09-05-09-(2)	River sand	Tributary	29.2190	92.0144	Siqunama, site 10 in Fig. 1B	This study
AY01-05-09-(1A)	River sand	Tributary	28.0054	94.2028	Subansiri River, site 11 in Fig. 1B	Cina et al. (2009)
SC03-26-08-(4)	River sand	Tributary	27.4517	94.2526	Subansiri River, site 12 in Fig. 1B	Cina et al. (2009)
Yalu-Siang-Brahmaputra Rivers						
DJG0804	River sand	Main trunk	29.3230	85.2424	Saga, site A in Fig. 1B	This study
AY09-08-08-(7)	River sand	Main trunk	29.3193	90.6864	Quxu, site B in Fig. 1B	This study
AY06-28-06-(1)	River sand	Main trunk	29.3228	91.0921	Gonggar, site C in Fig. 1B	Cina et al. (2009)
AY09-10-08-(12)	River sand	Main trunk	29.0747	92.7748	Gyaca, site D in Fig. 1B	This study
SC03-26-08-(6)	River sand	Main trunk	28.0768	95.3356	Siang River, site E in Fig.1B	Cina et al. (2009)
AY02-21-06-(2)	River sand	Main trunk	26.6108	92.8536	Brahmaputra River, site F in Fig.1B	Cina et al. (2009)
Eastern Himalayan foreland basin						
AY09-11-03-(1)	Sandstone	Dafla Fm.	27.1038	93.6247	Itanagar, site H-2 in Fig. 1B	Cina et al. (2009)
AY02-07-06-(13)	Sandstone	Subansiri Fm.	27.0163	93.6188	Itanagar, site H-2 in Fig. 1B	Cina et al. (2009)
AY02-07-06-(8)	Sandstone	Kimin Fm.	26.9816	93.6073	Itanagar, site H-2 in Fig. 1B	Cina et al. (2009)
AY02-12-06-(5)	Sandstone	Subansiri Fm.	27.0047	92.6417	Bhalukpong, site H-1 in Fig. 1B	Cina et al. (2009)

300 Ma, with age peaks of 35 Ma and 45 Ma (Fig. 3A). Zircon ages at 300–900 Ma account for 20% of the total dated grains. As the suture zone consists of Cretaceous to Eocene forearc sediments derived from the Lhasa terrane (Dürr, 1996), the younger than 300 Ma zircon grains were probably recycled from the forearc sediments rather than from igneous rocks of the Lhasa terrane.

Zedong Site

Sample AY09–10–08-(1) (site 3 in Fig. 1B) was collected from a south-flowing tributary of the Yalu River, ~5 km east of Zedong (~91.8°E). Zircon ages younger than 300 Ma with an age cluster of 40–85 Ma account for ~76% of the total dated grains (Fig. 3B).

Langxian Site

Sample AY09–11–08-(1) (site 4 in Fig. 1B) was collected from a south-flowing tributary near Langxian (~93.1°E). The zircon ages are dominated by clusters at 80–110 Ma and 300–370 Ma, accounting for 34% and 56%, respectively, of the total dated grains (Fig. 3C). When compared to the age results of other samples, the age cluster of 300–370 Ma is unique for this part of the southern Lhasa terrane (Fig. 3).

Layue Qu

Sample AY09–12–08-(1) (site 6 in Fig. 1B) was collected from the south-flowing Layue Qu (~94.9°E). Zircon ages are distributed mainly between 50 and 100 Ma, with a major 60 Ma peak and a minor 85 Ma peak (Fig. 3D). Nearly half of the dated grains yield ages from 750 Ma to 1600 Ma without any obvious peaks.

Long Tributaries in the Lhasa Terrane

Lhasa River

Sample AY09–08–08-(3) (site 2 in Fig. 1B) was collected from the southwest-flowing Lhasa River, ~50 km north of its confluence with the Yalu River (~90.9°E). Zircon ages of 13–206 Ma, with peaks at 65 Ma, 120 Ma, and 195 Ma, account for ~60% of the total zircon populations (Fig. 3E). The remaining ages are plotted between 420 Ma and 2.8 Ga. An age gap between 206 Ma and 420 Ma contrasts sharply to most age spectra of river sand obtained in this study (see Fig. 3 and following descriptions).

Nyingoh River

Sample AY09–11–08-(6) (site 5 in Fig. 1B) was from the Nyingoh River just north of its intersection with the Yalu River (~94.5°E). Zircon younger than 300 Ma only accounts for ~17% of the total dated grains (Fig. 3F). Age peaks at 35 Ma and 50 Ma and an age cluster between 190 Ma and 250 Ma are evident. A noticeable age gap exists between 85 Ma and 190 Ma (Fig. 3F). A significant fraction of older ages (~70%) between 500 Ma and 2.75 Ga was also obtained from this sample (Fig. 3F).

Parlung River

Sample AY09–12–08-(3) (site 7 in Fig. 1B) was collected from the Parlung River, ~30 km northwest of Bomi (~95.5°E). This sample is dominated by zircon ages between 100 Ma and 140 Ma (Fig. 3G). Grains younger than 200 Ma account for ~80% of the total grains. A major age peak occurs at 120 Ma, and a minor age peak occurs at 70 Ma. Zircon ages of 320–630 Ma account for ~18% of the total dated grains. A few zircon ages at 500 Ma, 900 Ma, 1.2 Ga, and ca. 1.7 Ga were also recorded.

Lohit River

Sample SC03–26–08-(5) (site 8 in Fig. 1B) was collected from the Lohit River, which flows through the Bomi-Chayu igneous belt into the Brahmaputra River (~94.9°E) (Cina et al., 2009). In this sample, zircon ages younger than 300 Ma account for 36% of the total dated grains and display a discontinuous distribution of ages from 50 Ma to 150 Ma, with a dominant peak at ca. 110 Ma (Fig. 3H). About 60% of the zircon grains show a continuous distribution of ages from ca. 1.0 Ga to ca. 3.3 Ga.

Yalu and Brahmaputra Tributaries across the Himalayan Orogen

Renbu Qu

Sample AY09–14–09-(4) (site 9 in Fig. 1B) was collected from the northwest-flowing Renbu Qu just south of its confluence with the

Zhang et al.
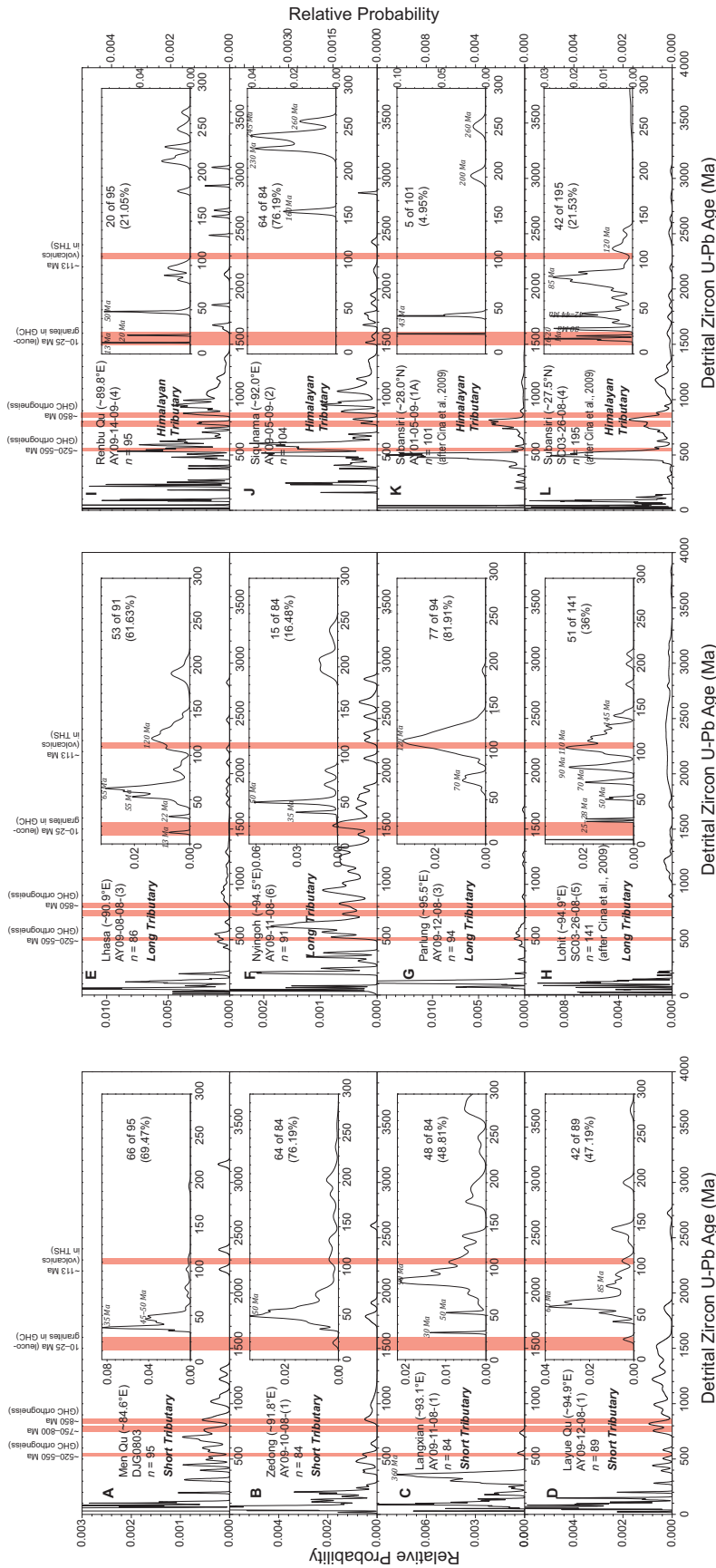
Figure 3. Relative probability plots of U-Pb ages (Ma) of detrital zircon from modern sand. They include samples collected from short rivers at Men Qu (A), Zedong (B), Langxian (C), and Layue Qu (D) and four from long rivers at Lhasa River (E), Nyingoh River (F), Parlung River (G), and Lohit River (H). Age spectra from river sand samples south of Yalu are shown for (I) Renbu Qu, (J) north-flowing Siqunama River; (K) at the middle reach of the Subansiri River, and (L) at the lower stream of the Subansiri River. Insets show detailed corresponding U-Pb age distributions at the age range of 0–300 Ma. Vertical red bands represent known ages of igneous rocks in the Yalu River basin. Age spectra for H, K, and L are quoted from Cina et al. (2009). GHC—Greater Himalayan Crystalline Complex; THS—Tethyan Himalayan Sequence.

Coupled U-Pb dating and Hf isotopic analysis of detrital zircon of modern river sands from the Yalu River

Yalu River (~89.8°E). In this sample, ~21% of dated zircon yielded ages younger than 300 Ma. Within this age range, there were three peaks, at ca. 12 Ma, 20 Ma, and 50 Ma (Fig. 3I). The first two peaks can be related to bedrock ages of Himalayan granites (e.g., Harrison et al., 1998), whereas the last peak is unique for the Gangdese zone in the Lhasa terrane. Since detrital-zircon ages at ca. 50 Ma are reported from nearby Eocene strata in the Himalayan orogen (Cai et al., 2011), the presence of 50 Ma zircon grains in the Renbu Qu is puzzling, and the source is unknown. Age clusters at 490–630 Ma and 870–1100 Ma can be correlated to bedrock ages of the Greater Himalaya (e.g., Gehrels et al., 2003; Yin et al., 2010a, 2010b), whereas the age cluster of 210–230 Ma may come from recycled detrital zircons of Triassic strata in the Tethyan Himalayan Sequence unit (Aikman et al., 2008). The 100 Ma age peak is most likely derived from zircon of the Gangdese igneous belt.

Siqunama River

Sample AY09–05–09-(2) (site 10 in Fig. 1B) was collected from the Siqunama River flowing northward into the Yalu River 25 km east of Zedong (~92.0°E). It yields ~7.7% of zircon ages younger than 300 Ma, in which a single zircon age of 160 Ma and an age cluster at 220–265 Ma are evident (Fig. 3J). Age clusters at 490–600 Ma and 880–1100 Ma were also detected.

Middle Stream of the Subansiri River

Sample AY01–05–09-(1A) (site 11 in Fig. 1B) from the middle reach of the southeast-flowing Subansiri River lies in the Greater Himalayan Crystalline Complex (~28.0°N) and was analyzed by Cina et al. (2009). Single zircon grains with ages at 22.8 Ma and 43 Ma were detected (Fig. 3K). The rest of the spectrum is dominated by age clusters at 450–550 Ma and 700–900 Ma.

Lower Stream of the Subansiri River

Sample SC03–26–08-(4) (site 12 in Fig. 1B), collected just south of the range front in Assam Valley (~27.5°N), was dated by Cina et al. (2009). The upper stream of the Subansiri River above this sample location drains the Tethyan Himalayan Sequence, Greater Himalayan Crystalline Complex, Lesser Himalayan Sequence, and Tertiary sediments in the Himalayan orogen. The sample yielded ages mostly between 70 and 100 Ma, with prominent peaks at 40–50 Ma and 80–90 Ma (Fig. 3L). The 80–90 Ma zircon population is not present in the sample from the middle stream of the Subansiri River (cf. Fig. 3K).

Yalu-Siang-Brahmaputra Rivers

Saga Site

Sample DJG0804 (site A in Fig. 1B) was collected from the Yalu River near Saga (~85.2°E). About 25% of the total dated zircon grains are younger than 300 Ma, and dominated by an age peak at ca. 45 Ma (Fig. 4A). Furthermore, 60% of the dated grains show a continuous distribution between 350 Ma and 1000 Ma with two minor age peaks at 500 Ma and 820 Ma.

Quxu Site

Sample AY09–08–08-(7) (site B in Fig. 1B) was collected from the south bank of the Yalu River near Quxu (~90.7°E), west of the confluence of the south-flowing Lhasa River and the Yalu River. This sample is dominated by zircon ages from 50 Ma to 60 Ma, with a peak at ca. 55 Ma (Fig. 4B). Zircon grains younger than 50 Ma are scattered between 15 and 40 Ma. A minor peak at ca. 500 Ma is also noticeable.

Gonggar Site

Detrital-zircon ages of sample AY06–28–06-(1) (site C in Fig. 1B) were reported by Cina et al. (2009), ~15 km east of Gonggar (~91.1°E). Zircon grains with ages younger than 120 Ma account for ~70% of the total dated grains. A dominant peak occurs at 50 Ma, and a minor peak occurs at 85 Ma (Fig. 4C). A small but statistically significant peak occurs at 500 Ma.

Gyaca Site

Sample AY09–10–08-(12) (site D in Fig. 1B) was collected from the right (south) bank of the main trunk of the Yalu River, ~20 km east of Gyaca (~92.8°E). Zircon grains with ages of 40–70 Ma account for nearly 40% of the total dated grains, and they show a dominant age peak at 50 Ma (Fig. 4D). In addition, 10% of the zircon grains have ages ranging from 87 to 112 Ma. For older zircons, 30% of the zircon grains are distributed between 450 and 1100 Ma, and the rest are scattered between 1300 and ca. 3.0 Ga.

Siang River

U-Pb ages of detrital zircon from sample SC03–26–08-(6) (site E in Fig. 1B) were reported by Cina et al. (2009) from Pasighat southeast of the eastern Himalayan syntaxis, ~30 km north of the confluence of the Lohit River (~95.3°E). About 25% of the dated grains are younger than 300 Ma (Fig. 4E). They show continuous distribution from 40 Ma to 90 Ma, with two age peaks at 42 Ma and 50 Ma. Older zircon grains are dominant (~70%), with a dominant age cluster centered at 500 Ma. The rest of the ages are scattered, with many results in the 800–1200 Ma, 1400–1700 Ma, and 2.7–3.8 Ga age ranges.

Brahmaputra River

U-Pb ages of detrital zircon from sample AY02–21–06-(2) (site F in Fig. 1B) were reported by Cina et al. (2009). This sample was collected from the Brahmaputra River just west of its confluence with the south-flowing Kameng River (~92.9°E). About 10% of the dated zircons have ages between 20 Ma and 140 Ma, with two age peaks at 30 Ma and 50 Ma (Fig. 4F). The zircon ages are continuous from 70 Ma to 140 Ma. The rest of the total dated grains (90%) show continuous distribution of ages between 400 Ma and 2.0 Ga, with three age peaks at 500 Ma, 850 Ma, and 1600 Ma. These ages can be correlated with the ages of orthogneiss in the eastern Himalaya (Yin et al., 2010b).

Hf ISOTOPIC VALUES OF DETRITAL ZIRCON

Short Rivers Traversing the Southern Gangdese Zone

Data points from four short river samples in the plot of U-Pb zircon ages (ZA) versus zircon Hf isotope values (ZH, i.e., ZA-ZH plot) (Fig. 5A) are indistinguishable in the range of $\varepsilon_{Hf}(t) = -2$ to $+5$ and zircon age = 35–240 Ma. Several isolated domains unique to each of the four samples can be identified under visual examination (Fig. 5A): (1) the Men Qu sample is characterized by a region with $\varepsilon_{Hf}(t)$ values from –11 to –1 and zircon ages of 35–50 Ma; (2) the Langxian sample is characterized by $\varepsilon_{Hf}(t)$ values of $+6$ to $+11$ and zircon ages of 180–220 Ma; (3) the Zedong sample is characterized by four domains, the largest of which has $\varepsilon_{Hf}(t)$ values of $+5$ to $+15$ and zircon ages of 40–100 Ma; and (4) the Layue Qu sample is characterized by $\varepsilon_{Hf}(t)$ values of –4 to –14 and zircon ages of 50–65 Ma.

Long Rivers Traversing the Entire Gangdese Zone

The data points from the four long river samples overlap in the ZA-ZH plots with $\varepsilon_{Hf}(t)$ values from 0 to –15 and zircon ages from 55 Ma to 240 Ma (Fig. 5B). Outside this overlapping region, isolated domains that are unique to each sample exist based on the available data: (1) the Lohit sample is characterized by very high $\varepsilon_{Hf}(t)$ values of +10 to +16 in the age range of 50–150 Ma; (2) the Parlung sample displays a cluster in the age range of 100–130 Ma with $\varepsilon_{Hf}(t)$ values of +1 to +5; (3) the Nyingoh and Lhasa River samples have their isolated domains next to each other in the age range of 40–65 Ma; and (4) the Lhasa River sample yields different $\varepsilon_{Hf}(t)$ values from the Nyingoh sample in the same age range.
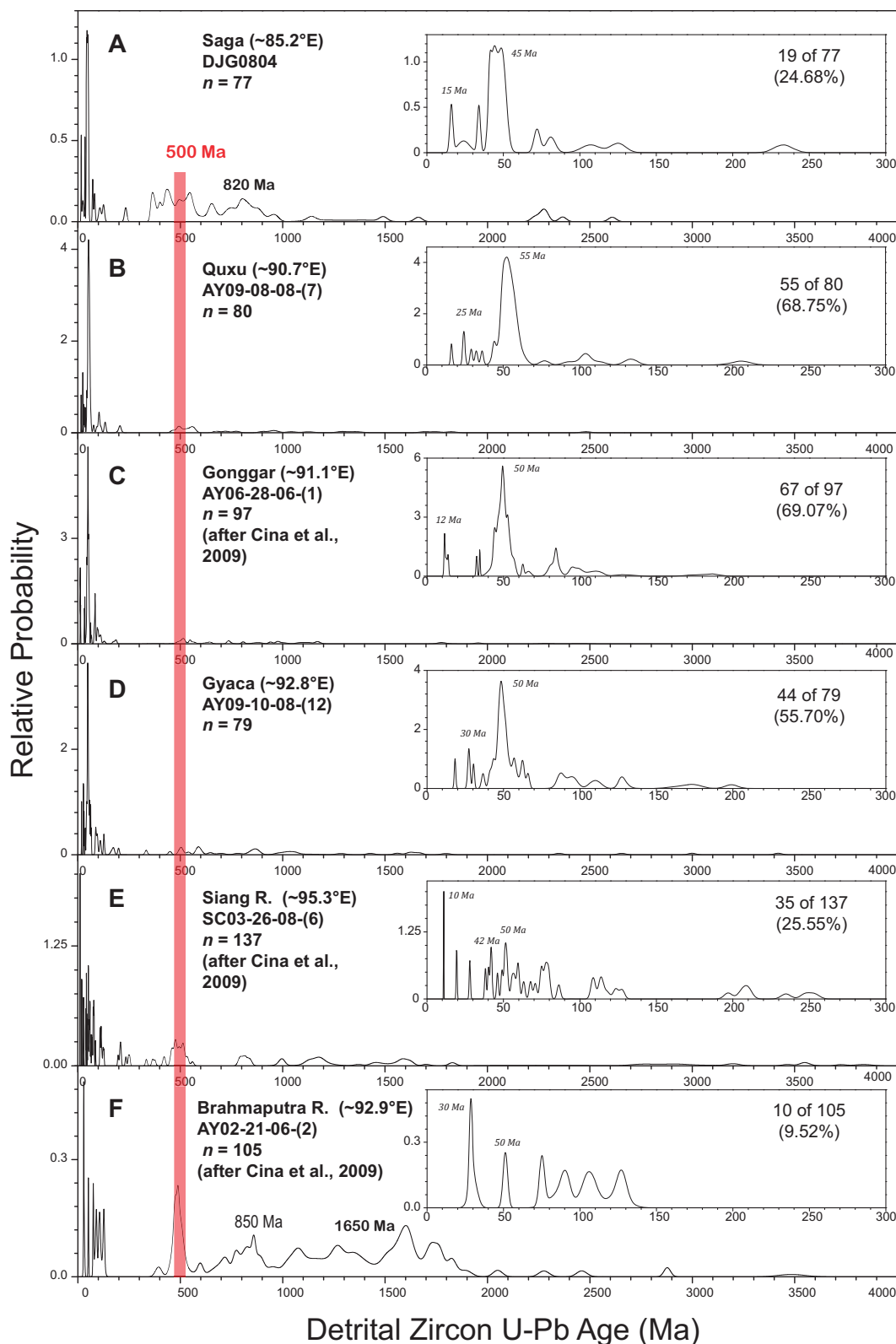
Figure 4. Relative probability plots of U-Pb ages (Ma) of detrital zircon from modern sand of the Yalu-Siang-Brahmaputra River for samples from (A) Saga, (B) Quxu, (C) Gonggar, (D) Gyaca, (E) Siang River, and (F) Brahmaputra River downstream. Insets display detailed U-Pb age spectra in the range of 0–300 Ma. Age spectra shown in A, B, and D are from this study, while those shown in C, E, and F are quoted directly from Cina et al. (2009).

Coupled U-Pb dating and Hf isotopic analysis of detrital zircon of modern river sands from the Yalu River
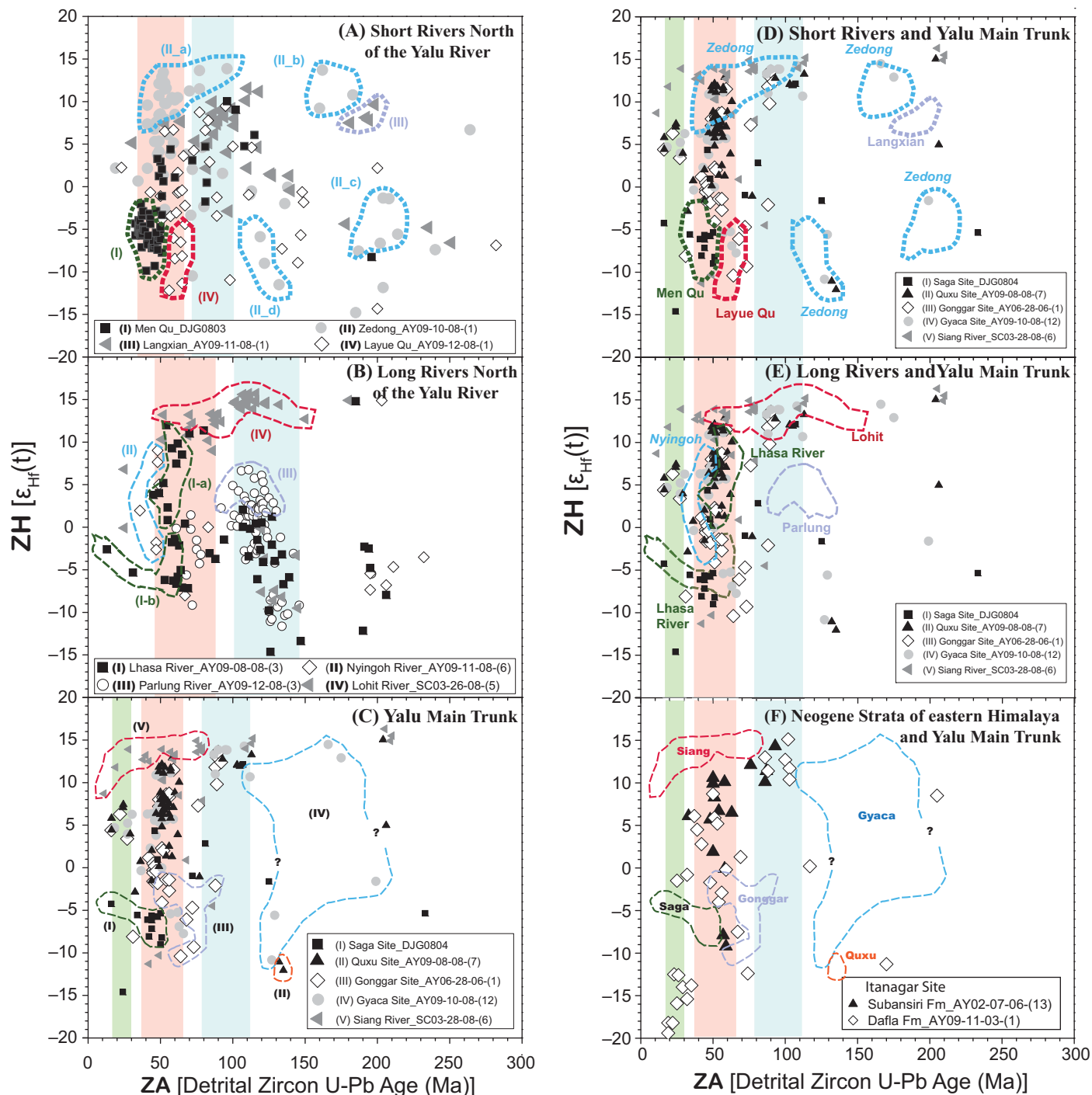
Figure 5. Lu-Hf isotopic values of detrital zircon versus detrital-zircon ages for the range of 0–300 Ma (ZA-ZH plots). (A) Samples from short rivers traversing the southern Lhasa terrane collected at Men Qu, Zedong, Langxian tributaries, and Layue Qu. (B) Samples from long rivers traversing the northern and southern igneous zones of the Lhasa terrane collected at Lhasa, Nyingoh, Parlung, and Lohit Rivers. (C) Samples from the main stream of the Yalu River at Saga, Quxu, Gonggar, and Gyaca and one sample from the Siang River. Regions outlined in A, B, and C mark zircon populations unique to particular samples. (D) Superposition of distinctive domains of the short-river samples over the ZA-ZH plots of the Yalu River samples. See text for details. (E) Superposition of distinctive domains of the long-river samples over the ZA-ZH plots of the Yalu River samples. (F) Superposition of distinctive domains of Yalu River samples over the ZA-ZH plots of Neogene sandstone samples from the eastern Himalayan foreland basin. The data sources for these samples are the same as those in Figures 3 and 4.

Yalu River

The dated five samples from the Yalu River are dominated by a 50 Ma age peak (Fig. 4), but the corresponding $\varepsilon_{Hf}(t)$ values vary (Fig. 5C). The upper-stream Saga sample has $\varepsilon_{Hf}(t)$ values of –10 to –5, while the downstream Quxu sample yields $\varepsilon_{Hf}(t)$ values of –2 to +13. The other three samples yield $\varepsilon_{Hf}(t)$ values of –11 to +13, with the Siang River sample mainly clustered around +13.

Although data points of the five Yalu River samples overlap with the $\varepsilon_{Hf}(t)$ values of 0 to +9 and zircon ages of 20–60 Ma, domains unique to each sample in the ZA-ZH plots can be recognized (Fig. 5C). The Siang River sample is characterized by high $\varepsilon_{Hf}(t)$ values of +13 to +15 in the age range of 20–60 Ma, whereas the Saga sample has $\varepsilon_{Hf}(t)$ values of –3 and –9 in the same age range. The Gonggar sample also defines a unique domain at 50–90 Ma with unique $\varepsilon_{Hf}(t)$ values. Due to large overlaps of the Gyaca and Quxu data points with other samples in the ZA-ZH plots, it is difficult to differentiate them in the ZA-ZH plots. A few data points in the age range of 110–200 Ma separate the Gyaca and Quxu samples from each other as well as from the other three samples (Fig. 5C), but this may not be statistically significant.

Comparison between Short River Samples and Yalu River Samples

We used ZA-ZH plots to examine the ways in which zircon ages and isotope signals from the short river samples are expressed in the samples from the Yalu River (Fig. 5D). The signature of zircon populations from the Zedong sample has a slight overlap with data points of the Quxu sample in the upper stream in the age range of 45–65 Ma and $\varepsilon_{Hf}(t)$ values of +5 to +12 in ZA-ZH plots (Fig. 5D). This implies that the Quxu sample in the upper stream carries signals of zircon populations that are similar to those recorded in the Zedong short river sample. Because of the overlap, we cannot tell whether the data points from the Siang River and Gyaca samples that fall in the Zedong domain were also derived in part from the Quxu segment of the Yalu River. Similarly, data points of the Gonggar and Gyaca overlap the Layue Qu domain (Fig. 5D). As Gonggar and Gyaca samples are located in the upper stream relative to the Yalu–Layue Qu confluence, the overlap indicates that similar zircon populations also exist in the upper-stream provenance that we did not sample. The nearly one-to-one correlation between the Men Qu domain and a cluster of data points from the Saga sample suggests that the Saga River sand contains a distinctive zircon population with provenance from the Men Qu drainage basin.

Comparison between Long River Samples and Yalu River Samples

In the ZA-ZH plot, the Lhasa River domain contains the data points of the Saga and Quxu samples collected from the upper-stream Yalu River (Fig. 5E), which indicates that similar or the same provenance domains have also contributed to the zircon populations at these two upper-stream sites. We find that the distinctive domain of the Parlung River sample is not expressed in any of the main trunk samples of the Yalu River. The Lohit domain contains data points from Gyaca, Quxu, and Gonggar, suggesting that the upper stream of the Yalu River also contains similar provenance domains unique to the Lohit River zircon. The Nyingoh domain contains data points from the Quxu, Gonggar, and Gyaca samples (Fig. 5E), indicating that the upper-stream Yalu River has received detritus from provenances similar to those of the Nyingoh River basin. We note that the Nyingoh domain does not contain data points corresponding to the Saga and Siang River samples.

Comparison between Yalu River Samples and Foreland Basin Samples

Using the results of Cina et al. (2009) on the age and Hf isotope composition of detrital zircon from Neogene sediments of the eastern Himalayan foreland basin, we are able to compare the zircon populations between Yalu River samples and Neogene sandstone samples in a ZA-ZH plot (Fig. 5F). We find that the Siang River, Gyaca, and Quxu domains do not overlap any data points of the Neogene foreland-basin samples. In contrast to the lack of correlation in detrital-zircon populations between the Siang River and foreland-basin samples, a unique zircon population from the Gonggar sample site, defined by the Gonggar domain in Figure 5F, overlaps the data points from sandstone samples of the Dafla and Subansiri Formations in the eastern Himalayan foreland.

MODAL COMPOSITION OF RIVER SAND

Short Rivers North of the Yalu River

Modal composition of the Men Qu sample (DJG0803; site 1 in Fig. 1B) plots in the field of a dissected arc (Fig. 6; Table 2). Men Qu, located north of the Yalu River, drains the Himalayan orogen and the Indus-Tsangpo suture zone. Its modal composition reflects these source regions characterized by recycled arc rocks in the suture zone.

The Zedong sample (AY09–10–08-[1] at site 3 in Fig. 1B) was collected from a tributary that drains the southern Lhasa terrane. The catchment area exposes Jurassic–Cretaceous sedimentary and volcanic strata intruded by Cretaceous–Early Tertiary plutons (Yin et al., 1999; Harrison et al., 2000; Pan et al., 2004). The high proportion of lithic fragments (Table 2) may be explained by the widely occurring, easily erodible sedimentary and volcanic rocks. The Zedong sample plots in the field of a transitional arc (Fig. 6).

The Langxian sample (AY09–11–08-[1] at site 4 in Fig. 1B) plots in the field of a dissected arc (Table 2; Fig. 6). This is consistent with the fact that the tributary drains exclusively plutonic rocks of the Gangdese arc (Harrison et al., 2000; Pan et al., 2004).

The Layue Qu sample (AY09–12–08-[1] at site 6 in Fig. 1B) plots in the field of a dissected arc (Table 2; Fig. 6). This is consistent with the tributary draining a highly exhumed segment of the southern Gangdese arc near the eastern Himalayan syntaxis (Ding et al., 2001; Pan et al., 2004).

Long Rivers North of the Yalu River

The Lhasa River sample (AY09–08–08-[3] at site 2 in Fig. 1B) plots in the field of a transitional arc (Fig. 6; Table 2). This may reflect the fact that Mesozoic and Early Tertiary volcanic rocks are extensively exposed in the source region of the Lhasa River in the northern Lhasa terrane (Pan et al., 2004). As a result, volcanic detritus dominates sediments in the Lhasa River.

The Nyingoh River traverses the eastern end of the Gangdese arc and extends into the northern zone of the Lhasa terrane. Sample AY09–11–08-(6) from the river sand (site 5 in Fig. 1B) plots near the boundary between a recycled orogen and a dissected arc (Fig. 6; Table 2).

The northwest-flowing Parlung River drains the northernmost portion of the Bomi-Chayu igneous belt (Fig. 1B). Sample AY09–12–08-(3) from the river sand (site 7 in Fig. 1B) plots close to the boundary between a recycled orogen and a dissected arc (Fig. 6; Table 2).

Main Trunk of the Yalu River

Modal composition of Yalu River sand varies spatially (Fig. 6C; Table 2). This is indicated by a dramatic increase in the percentage of lithic fragments downstream along the river, from 40%–45% at Saga and Quxu to 58% at Gyaca. The Saga sample plots in the field of a recycled orogen (Fig. 6). As the Lhasa terrane is dominated by the Gangdese batholith, it is more likely that the Tethyan Himalayan Sequence

Coupled U-Pb dating and Hf isotopic analysis of detrital zircon of modern river sands from the Yalu River
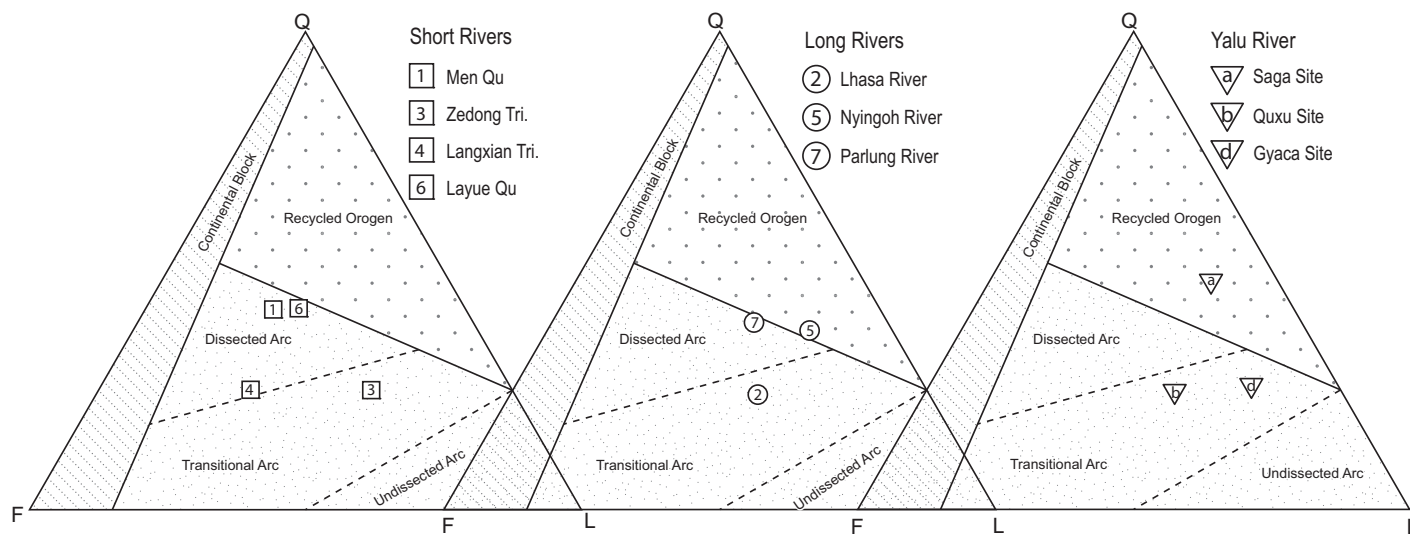
Figure 6. Q-F-L diagram of modern sand from short rivers and long rivers across the Lhasa terrane and from the main stream of the Yalu River.

TABLE 2. MODAL COMPOSITION OF RIVER SANDS

Sample name	Sample number	Component number				Component percentage (%)		
		Q	F	L	Total	Q	F	L
Short rivers north of the Yalu River								
Men Qu	DJG0803	132	111	74	317	41.6	35.0	23.3
Zedong	AY09-10-08-(1)	81	84	162	327	24.8	25.7	49.5
Langxian	AY09-11-08-(1)	80	153	89	322	24.8	47.5	27.6
Layue Qu	AY09-12-08-(1)	155	112	103	370	41.9	30.3	27.8
Long rivers north of the Yalu River								
Lhasa River	AY09-08-08-(3)	75	97	140	312	24.0	31.1	44.9
Nyingoh River	AY09-11-08-(6)	115	46	146	307	37.5	15.0	47.6
Parlung River	AY09-12-08-(3)	126	78	118	322	39.1	24.2	36.6
Main trunk of the Yalu River								
Saga site	DJG0804	174	44	146	364	47.8	12.1	40.1
Quxu site	AY09-08-08-(7)	95	116	173	384	24.7	30.2	45.1
Gyaca site	AY09-10-08-(12)	78	47	175	300	26.0	15.7	58.3

detrital components from banks and tributaries. In addition, erodibility, areal coverage, drainage geometry, and lithology may also control the composition of river sand. Next, we quantify variations in detrital-zircon populations (1) between the source regions and the fluvial delivery systems, (2) within the fluvial delivery systems, and (3) between the fluvial delivery systems and the sink regions. This is accomplished by using combined detrital-zircon U-Pb ages, Hf isotope compositions (Figs. 4 and 5), and bedrock geology (Fig. 7). The comparison is conducted by employing cumulative probability plots and two-sample Kolmogorov-Smirnov (K-S) tests (Fig. 8; Table 3).

Comparison between Source Regions and Fluvial Delivery Systems

We compare U-Pb age spectra and $\varepsilon_{Hf}(t)$ values of our river sand samples with their corresponding provenances. The drainage basin of the Lhasa River was selected for this purpose because its bedrock geology and age distributions are best known in Tibet (e.g., Ji et al., 2009, 2010; Zhu et al., 2009a, 2009b, 2011; He et al., 2007; Mo et al., 2007, 2009; Leier et al., 2007; Lee et al., 2009) (Fig. 7A).

The U-Pb zircon age spectra and the corresponding $\varepsilon_{Hf}(t)$ values from plutonic rocks, volcanic rocks, and sedimentary strata in the Lhasa River catchment are summarized in Figures 7B–7E. There are far more age determinations of plutonic rocks ($n = 711$) than those of volcanic ($n = 158$) and sedimentary ($n = 251$) rocks in the Lhasa River basin (Fig. 7B). To get the synthetic age signature and make a better comparison, we not only plot directly the available

(THS) was the main source of the sampled sand. This interpretation is consistent with the fact that the Yalu River flows entirely within the Himalayan orogen over a distance of 200 km where the Saga sample was collected (site A in Fig. 1B). This interpretation implies that despite the presence of tributaries from the left (north) bank that deliver detritus from the Lhasa terrane to the Yalu River, bank erosion along the main course of the Yalu River may have contributed most of the sediment load in the river.

The Quxu and Gyaca samples (sites B and D in Fig. 1B) were collected along the Yalu River where it follows the Indus-Tsangpo suture zone. The modal compositions of the two samples are plotted in the field of a transitional arc (Fig. 6). We note that near the Quxu and Gyaca sites, the Gangdese arc exposes mostly plutonic rocks (>80% in areal extent), with minor strips of Triassic to Cretaceous strata (Harris et al., 1988; Yin et al., 1994, 1999; Pan et al., 2004). Thus,

the relatively high lithic contents of the two samples may have been induced by contributions from the more easily erodible Himalayan sources.

VARIATION OF U-Pb AGES FROM SOURCE TO SINK THROUGH FLUVIAL DELIVERY SYSTEMS

The Yalu River and its southern extension into the Siang and Brahmaputra Rivers form a detrital delivery system that links the source regions across the Lhasa terrane and the Himalayan orogen with the sink regions in the Himalayan foreland (Fig. 1C). Ideally, the detritus from the source regions is completely transported to the sink regions (i.e., the foreland basin and continental margins through which the river flows or in which it terminates). In reality, the composition of the river sand changes downstream along the Yalu River due to reworking of older stranded deposits and addition of new

data (type I), but also normalize the age spectrum of each type of rock according to their relative exposure areas (type II): 28% for plutonic rocks, 19% for volcanic rocks, and 58% for sedimentary rocks (Figs. 7C and 7E). The latter bears an implied assumption that the production of zircon and the distribution of zircon populations are spatially uniform, which is clearly not the case. Given the lack of systematic sampling and dating of bedrock, this approach should be treated as a first-order estimate only.

The plutonic rocks within the Lhasa drainage areas are dominated by the Gangdese batholith, and as a result they display age peaks at 18 Ma, 50 Ma, and 75 Ma, characteristic of the southern igneous zone of the Lhasa terrane (Fig. 7B). The corresponding $\varepsilon_{Hf}(t)$ values are +1.5 to +11.5, –1 to +14, and +10 to +13, respectively (Fig. 7D). Volcanic rocks in the Lhasa River drainage area include the Lower Jurassic Yeba Group, the Lower Cretaceous Sangri Group, and the Upper Cretaceous to Lower Tertiary Linzizong Group (He et al., 2007; Lee et al., 2007, 2009; Zhu et al., 2008c, 2009c). They show one main age cluster at 40–70 Ma and two minor peaks at 135 Ma and 170 Ma (Fig. 7B). The corresponding $\varepsilon_{Hf}(t)$ values are between 0 and +11 for 40–70 Ma zircon and at +13 for 135 Ma zircon (Fig. 7D). Detrital-zircon grains from Carboniferous to Eocene sedimentary rocks are dominated by two age peaks at 120 Ma and 140 Ma (Leier et al., 2007; Kapp et al., 2007b) (Fig. 7B). They also display continuous distributions between 170 Ma and 250 Ma and between 260 Ma and 290 Ma. A minor age peak at 55 Ma is also detected in Eocene strata (Fig. 7B). When combined together, we obtained a synthetic age spectrum of all three types of bedrock from the Lhasa River drainage area, which shows three age peaks at 50 Ma, 120 Ma, and 140 Ma (Fig. 7C). A prominent age gap occurs between 160 Ma and 185 Ma for the bedrock (Fig. 7B).

The sample from Lhasa River sand (AY09–08–08–[3] at site 2 in Figs. 1B and 7A) exhibits age peaks at 52 Ma, 65 Ma, and 115 Ma (Fig. 7B), corresponding closely with the age peaks of the bedrock. The strength of the 52 Ma peak from detrital zircon is weaker than that of the same age peak for the plutonic rocks (Fig. 7C).

A comparison of zircon ages from source rocks and detrital-zircon ages of Lhasa River sand suggests: (1) there are large numbers of zircon grains from the Lhasa River sample that do not display zircon ages of the bedrock (i.e., domain III in Fig. 7D); (2) distinctive zircon populations detected from bedrock are not represented in detrital-zircon ages of the Lhasa River sand sample (domains I-a, I-b, and II); and (3) the overlapping domain defined by data points from the Lhasa River sample and bedrock is restricted within a cluster that has $\varepsilon_{Hf}(t)$ values between 0 and +15 and detrital-zircon ages between 35 Ma and 90 Ma (Fig. 7D). The lack of zircon populations recorded in the river sand in bedrock data may be explained in three ways. First, it is possible that the sampling of bedrock across the Lhasa River basin is highly biased by the accessibility provided by the roads and exposure conditions. Second, it is also possible that the source rocks that generated the unmatched zircon populations in the Lhasa River sand have been eroded away or buried in recent times. Third, some of the dated sand grains may have been transported via wind over a long distance, and their source areas may be located completely outside the Lhasa River drainage basin. This possibility raises particular concerns, as the cornerstone of detrital-zircon provenance analysis is based on the assumption that all detritus is transported by fluvial systems linking source rocks to the terminal sedimentary basins. This possibility may be tested in the future by examining zircon ages as a function of grain size. Fourth, rapid delivery of zircon populations from highly localized sources that are unrepresentative of the overall bedrock age distribution could also bias the sampling of zircon ages from river sand. For example, occurrence of a landslide at a narrow river gorge could temporarily overwhelm the detrital composition of the river sand. Unfortunately, the time scale for sand mixing due to landsliding is currently unknown.

The lack of matching bedrock zircon populations in the Lhasa River sample (cf. Fig. 7D) is at present difficult to interpret, as we are limited to data from a single sample. However, the lack of volcanic zircons with high $\varepsilon_{Hf}(t)$ values of 10–16 in the age range of 115–140 Ma in the river sand may be caused by the downstream dilution effect (see more detailed discussion on this issue in the following sections) (Stewart et al., 2008; Cina et al., 2009), low erodibility of volcanic rocks, and higher mechanical strength that prevents volcanic clasts from disintegrating into single zircon grains in river sand. The lack of young zircon with high $\varepsilon_{Hf}(t)$ values of 0 to +13 in the age range of 15–25 Ma in the Lhasa River sample could be caused by extremely small outcrop areas (mostly <10 km^2) or subdued relief of the exposures of these rock types, yielding slower rates of erosion (e.g., Finnegan et al., 2008).

Variations within Fluvial Delivery Systems

Two samples collected by Cina et al. (2009) from the Subansiri River display similar age spectra older than 230 Ma (Figs. 3K and 3L). For the middle-stream sample collected in a region where the river flows over the Greater Himalayan Crystalline Complex unit (sample from site 11 in Fig. 1B), the sample yields 22.8 Ma zircon age compatible with the known ages of Greater Himalayan Crystalline Complex leucogranites in the area (Yin et al., 2010a). It also contains 43 Ma zircon grains, consistent with the presence of 44 Ma granites in the upper catchment of the Subansiri River (Aikman et al., 2008). The lower-stream sample again yields 16–20 Ma, 30 Ma, and 42–44 Ma zircon grains (Fig. 3L). However, the age spectrum of the lower-stream sample also displays a completely different age distribution between 60 and 140 Ma from that of the upper stream sample (Fig. 3L and sample site 12 in Fig. 1B; cf. Fig. 3K). The zircon population is similar to that of the Neogene

Figure 7. (A) Simplified geological map of the Lhasa River catchment area modified from Pan et al. (2004). The topographic base map was adopted from the Global Multi-Resolution Topography (GMRT) by Ryan et al. (2009) from http://www.geomapapp.org. The published age data are based on Ji et al. (2009), Ji (2010), Zhu et al. (2008c, 2009c, 2011), Mo et al. (2007), Lee et al. (2007, 2009), He et al. (2007), Leier et al. (2007), Kapp et al. (2007b), and Chung et al. (2009). (B) Relative probability plots of plutonic, volcanic, and sedimentary rocks in the Lhasa River drainage basin. They are compared against the relative probability plot of detrital-zircon ages of the Lhasa River sample collected at location 2 in Figures 1B and 7A. (C) Synthetic relative probability of bedrock ages from the Lhasa River basin: (I) plotted directly from the available dates, and (II) plotted by weighting the areas of plutonic, volcanic, and sedimentary rocks in the river basin. These two plots are further compared with that of the Lhasa River sample collected at location 2 shown in Figure 1B and 7A. (D) The U-Pb zircon age and Hf isotopic results (ZA-ZH plot) for the plutonic and volcanic rocks from the Lhasa River basin and the Lhasa River sand. (E) The cumulative probability plots for types I and II bedrock zircon ages available and the Lhasa River sand (Figs. 1B and 7A). Two-sample K-S test of zircon U-Pb ages between type II bedrocks and Lhasa River sand indicates they do not belong to the same zircon population. See text for detailed discussion of the similarities and differences between the bedrock and river sand zircon populations.

Coupled U-Pb dating and Hf isotopic analysis of detrital zircon of modern river sands from the Yalu River
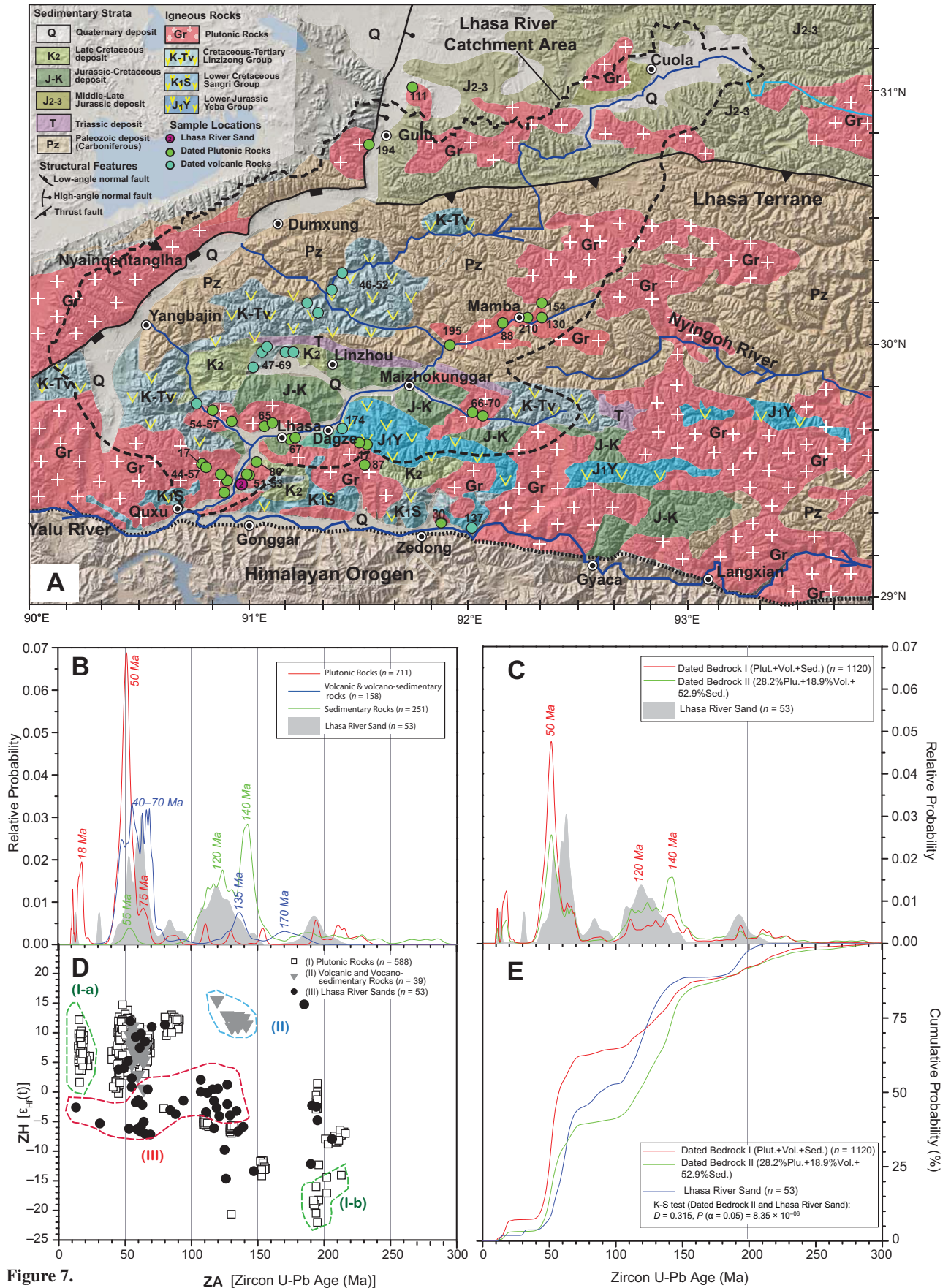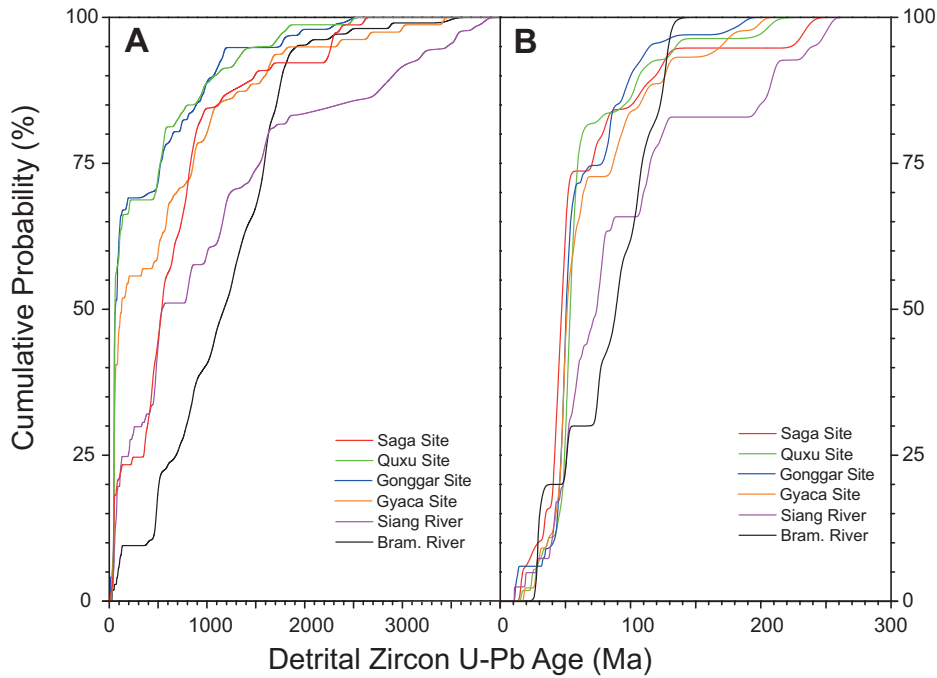
Figure 7.

Figure 8. Cumulative probability plots of modern river sand from the Yalu River at the age range of 0–4000 Ma (A) and the age range of 0–300 Ma (B).

is a useful nonparametric test for the equality of continuous one-dimensional probability distributions of two samples. The tested samples are typically displayed in cumulative probability diagrams (Fig. 8), and their largest vertical difference in the plot is defined as the D value (Table 3). Typically, a threshold value of $\alpha = 0.01$ or 0.05 is set. That is, if D value is $> D_{critical}$ ($\alpha = 0.05$), the null hypothesis (H_0) that the two samples are drawn from the same population can be rejected. $D_{critical}$ can be calculated by $D_{critical} = 1.36([N_1 + N_2]/[N_1N_2])^{1/2}$ for $\alpha = 0.05$, where N_1 and N_2 are the number of dated zircons from two samples for comparison. In this study, we dated ~100 zircon grains for each sample, and the corresponding critical value for D is $D_{critical} = 0.192$. The P value in K-S tests denotes the threshold of the significance level at which the null hypothesis (H_0) can be accepted. That is, P value must be greater than 0.05 when two samples are from the same parent distribution at 95% confidence level.

Table 3A displays comparison of age spectra of all samples. We also isolate the age range of 0–300 Ma for comparison to highlight the presence and absence of detrital-zircon components from the Lhasa terrane (cf. Table 3B). The (D, P) values for the age range of 0–300 Ma between the spectrum of the Saga sample and that of the Quxu, Gonggar, Gyaca, Siang River, and Brahmaputra River samples are (0.357, 0.055), (0.230, 0.411), (0.237, 0.447), (0.416, 0.022), and (0.460, 0.124), respectively. The large P values (i.e., >0.05) imply that the age spectra of the Quxu, Gonggar, Gyaca, and Brahmaputra

foreland sediments in the Himalaya and was interpreted to have resulted from recycling of the poorly consolidated Tertiary strata (Cina et al., 2009). These observations indicate that subtle upper-stream age signals can be effectively carried downstream via fluvial transport along the Subansiri River. However, the relative proportion of various zircon age populations varies depending on detrital fluxes from local sources.

At a much larger scale, we compared six samples collected from the Yalu River using two-sample Kolmogorov-Smirnov (K-S) tests to determine the ways in which zircon populations vary along a major river. The K-S statistic

TABLE 3A. *P* AND *D* VALUES USED IN TWO-SAMPLE KOLMOGOROV-SMIRNOV (K-S) TESTS (0–4000 Ma)

D value / *P* value	Saga site	Quxu site	Gonggar site	Gyaca site	Siang River	Brah. River	Itanagar (H-2) Dafla Fm.	Subansiri Fm.	Kimin Fm.	Bhalukpong (H-1) Subansiri Fm.
Saga site	–	0.453	0.475	0.343	0.268	0.441	0.192	0.217	0.222	0.204
Quxu site	2.01 × 10⁻⁰⁷	–	0.120	0.151	0.441	0.594	0.559	0.455	0.526	0.336
Gonggar site	8.05 × 10⁻⁰⁹	**5.50 × 10⁻⁰¹**	–	0.161	0.474	0.618	0.588	0.476	0.552	0.359
Gyaca site	2.04 × 10⁻⁰⁴	**3.22 × 10⁻⁰¹**	**2.09 × 10⁻⁰¹**	–	0.333	0.495	0.453	0.337	0.419	0.225
Siang River	1.65 × 10⁻⁰³	6.00 × 10⁻⁰⁹	1.60 × 10⁻¹¹	3.01 × 10⁻⁰⁵	–	0.276	0.219	0.156	0.143	0.211
Brah. River	6.37 × 10⁻⁰⁸	2.34 × 10⁻¹⁴	3.88 × 10⁻¹⁷	4.98 × 10⁻¹⁰	2.41 × 10⁻⁰⁴	–	0.380	0.296	0.252	0.485
H-2 Dafla Fm.	2.79 × 10⁻⁰²	1.55 × 10⁻¹⁶	6.94 × 10⁻²¹	6.78 × 10⁻¹¹	5.30 × 10⁻⁰⁴	1.74 × 10⁻⁰⁹	–	0.155	0.163	0.318
Sub. Fm.	1.14 × 10⁻⁰²	1.64 × 10⁻¹⁰	4.85 × 10⁻¹³	6.52 × 10⁻⁰⁶	4.13 × 10⁻⁰²	1.46 × 10⁻⁰⁵	1.35 × 10⁻⁰²	–	0.093	0.197
Kimin Fm.	7.89 × 10⁻⁰³	2.64 × 10⁻¹⁴	5.92 × 10⁻¹⁸	3.88 × 10⁻⁰⁹	**6.74 × 10⁻⁰²**	2.93 × 10⁻⁰⁴	5.95 × 10⁻⁰³	**3.57 × 10⁻⁰¹**	–	0.286
H-1 Sub. Fm.	4.69 × 10⁻⁰²	6.26 × 10⁻⁰⁵	3.68 × 10⁻⁰⁶	1.95 × 10⁻⁰²	9.33 × 10⁻⁰³	2.64 × 10⁻¹¹	7.26 × 10⁻⁰⁷	9.64 × 10⁻⁰³	1.74 × 10⁻⁰⁵	–

Note: The software used, K-S test 1.0.xls, is from the University of Arizona.

TABLE 3B. *P* AND *D* VALUES USED IN TWO-SAMPLE K-S TESTS (0–300 Ma)

D value / *P* value	Saga site	Quxu site	Gonggar site	Gyaca site	Siang River	Brah. River	Itanagar (H2) Dafla Fm.	Subansiri Fm.	Kimin Fm.	Bhalukpong (H-1) Subansiri Fm.
Saga site	–	0.357	0.230	0.237	0.416	0.460	0.251	0.487	0.557	0.171
Quxu site	**0.055**	–	0.185	0.156	0.376	0.517	0.273	0.427	0.497	0.210
Gonggar site	**0.411**	**0.250**	–	0.092	0.355	0.445	0.254	0.413	0.502	0.148
Gyaca site	**0.447**	**0.589**	**0.978**	–	0.279	0.427	0.231	0.324	0.417	0.133
Siang River	0.022	0.003	0.003	**0.073**	–	0.204	0.250	0.129	0.150	0.264
Brah. River	**0.124**	0.022	**0.064**	**0.103**	**0.891**	–	0.280	0.165	0.242	0.418
H-2 Dafla Fm.	**0.377**	**0.054**	**0.068**	**0.196**	**0.146**	**0.550**	–	0.328	0.316	0.212
Sub. Fm.	0.003	0.000	0.000	0.016	**0.854**	**0.978**	0.015	–	0.110	0.333
Kimin Fm.	0.001	0.000	0.000	0.002	**0.790**	**0.751**	0.042	**0.967**	–	0.406
H-1 Sub. Fm.	**0.846**	**0.258**	**0.642**	**0.852**	**0.120**	**0.122**	**0.309**	0.016	0.004	–

Note: The software used, K-S test 1.0.xls, is from the University of Arizona.

River samples belong to the same population as the age spectrum of the Saga sample. The differences in the *D* values also inform us that the age spectrum of the Saga sample is more similar to those of the Quxu, Gonggar, and Gyaca samples. However, it differs significantly from the age spectra of the Siang River and Brahmaputra River samples. In contrast, the *D* value between the age spectra of the Siang River and Brahmaputra River samples is only 0.204, i.e., much smaller than the values of *D* = 0.416 between the Saga and Siang samples and *D* = 0.460 between the Saga and Brahmaputra samples (Table 3B). The closer similarity of the age spectra for the Siang River and Brahmaputra River samples is also indicated by their high *P* value of 0.891 in the age range of 0–300 Ma. Table 3B also shows that the age spectra of the Gyaca and Gonggar samples are very similar, with a low *D* value of 0.156 and a high *P* value of 0.978. The age spectra of the Gonggar and Quxu samples are also similar, with a *P* value of 0.598, but yield a higher *D* value of 0.185 for the age range of 0–300 Ma.

The differences in detrital-zircon age spectra may also provide clues on potential provenances of the samples collected from the Yalu River. The Yalu River at the Saga site (site A in Fig. 1B) receives detritus from the western segment of the southern Lhasa terrane (provenance domain S1) and the Himalayan orogen (provenance domain S5) (Figs. 1B and 1C). The age spectrum of the Saga sample at the range of 0–300 Ma resembles those of the S1 domain (Fig. 4A), with the corresponding $\varepsilon_{Hf}(t)$ values similar to those obtained from the Men Qu sample collected ~70 km upstream north of the Yalu River (cf. Fig. 5A and Fig. 5C). The age spectrum older than 300 Ma is similar to the S5 domain, as indicated by the continuous distribution of zircon ages from 350 Ma to 1000 Ma (Fig. 4A).

The Yalu River at Quxu site receives detritus from the Lhasa terrane (provenance domains S1, S2, and S4) and the Himalayan orogen (provenance domain S5) (Figs. 1B and 1C). The whole age spectrum for the Quxu sample from the Yalu River is easily distinguished from that of the Saga sample due to an obvious increase from 25% to 70% of the total zircon grains with ages at 0–300 Ma (Table 3B; Fig. 8). This difference might result from a variation of provenance along the Yalu River. The main age clusters and the corresponding $\varepsilon_{Hf}(t)$ values for the Quxu sample are similar to those of the southern Lhasa terrane, with little hint for a contribution of detritus from the northern Lhasa terrane (Figs. 2F and 2G; cf. Figs. 4B and 5).

The age spectrum of the Gonggar sample may be indistinguishable from the Quxu sample by its slight shift of the most dominant age peak from 55 Ma to 50 Ma and a discontinuous age distri-

bution in the range of 10 Ma to 40 Ma (cf. Fig. 4C and Fig. 4B). However, the overall cumulative probability plots of the two samples are very similar (Table 3B; Fig. 8). The $\varepsilon_{Hf}(t)$ values of the Gonggar sample are similar to those of the Lhasa River sample located ~40 km upstream (Figs. 5B and 5C). Although the Lhasa River carries the age and isotopic signatures of the northern Lhasa terrane, the Yalu River sample at the Gonggar site does not (Figs. 4C and 5C; cf. Figs. 2A and 2F), suggesting that the northern Lhasa detrital-zircon signatures are completely diluted in the Yalu River at the Gonggar site. The Yalu River sample collected at Gyaca displays a similar age spectrum to that obtained from the Gonggar sample, but the relative proportion of detrital zircon in the age range of 0–300 Ma decreases from 70% to 56% (Figs. 4C, 4D, and 8).

South of the eastern Himalayan syntaxis, after the horseshoe turn of the Yalu River, the Siang River flows entirely within the Himalayan orogen. As a result, samples from it and its connected Brahmaputra River display dramatically different age spectra from those obtained from samples along the east-flowing Yalu River (Fig. 8). Specifically, the Siang and Brahmaputra River samples at sites E and F in Figure 1B have a lower cumulative probability in detrital-zircon ages younger than 200 Ma in comparison to the age spectra obtained from the upper stream of the Yalu River (Fig. 8). Although the age spectrum of the Sing River sample is broadly similar to that of the Gyaca sample in the upper stream, the proportion of the 0–300 Ma detrital-zircon component decreases from ~56% to 26% (Figs. 4D and 4E). The sample from the Brahmaputra River includes less than 10% of detrital zircons that are younger than 300 Ma (Fig. 4F), which requires further dilution of the young zircon component in the river sand.

Variations between Delivery Systems and Sinks

We made quantitative comparisons between the age spectra of Neogene–Quaternary sandstone samples from the eastern Himalayan foreland basin (Cina et al., 2009) and the age spectra of Yalu River sand samples obtained from this study. The Neogene–Quaternary units in the eastern Himalayan foreland basin consist of four formations (Kumar, 1997): the early and middle Miocene Kimi Formation, the late Miocene Dafla Formation, the late Miocene (?) and early Pliocene Subansiri Formation, and the late Pliocene to Quaternary Kimin Formation. A regional Cenozoic thrust juxtaposes the Dafla strata over Subansiri strata (Yin et al., 2010a).

The age spectrum of the Dafla sample from Itanagar (sample location H2 in Fig. 1B) is

indistinguishable from the age spectra of the Saga, Quxu, Gonggar, and Gyaca samples from the Yalu River (Fig. 9), with *D* values ranging from 0.231 to 0.273 for the age range of 0–300 Ma (Table 3B). The age spectra of the overlying Subansiri and Kimin samples from Itanagar (site H-2 in Fig. 1B) are markedly different from the Dafla sample at the range of 0–300 Ma, with corresponding larger *D* values of 0.328 and 0.316. When comparing them against the samples from the Yalu, Siang, and Brahmaputra River samples, we find that the age spectrum of the Subansiri Formation sample is more similar to the spectra of the Saga (*D* = 0.217) and Siang River (*D* = 0.156) samples than the age spectra of the Quxu (*D* = 0.455), Gonggar (*D* = 0.476), Gyaca (*D* = 0.337), and Brahmaputra River (*D* = 0.296) samples for the entire age spectra (Table 3A). For the Kimin sample from Itanagar, its spectrum is most similar to the age spectra of the Siang River (*D* = 0.143) and Saga (*D* = 0.222) samples but drastically different from the age spectra of the Quxu, Gonggar, and Gyaca samples, which have *D* values of 0.526, 0.552, and 0.419, respectively, for the whole age range (Table 3A). The similarities of age spectra between the Saga/Siang River samples and Subansiri/Kimin samples may be explained by the fact that both the Yalu River at the Saga site and the Siang River flow across the Himalayan orogen and derive most of their detritus from it.

In the Bhalukpong area, ~120 km to the east (site H-1 in Fig. 1B), the age spectrum of a Subansiri sample is more similar to the age spectra of the Gonggar (*D* = 0.148) and Gyaca (*D* = 0.133) samples from the Yalu River than to the age spectra of the Siang (*D* = 0.264) and Brahmaputra River (*D* = 0.418) for the age range of 0–300 Ma (Table 3B). This similarity in age spectra between the Yalu River samples and the Subansiri sandstone sample in the Himalayan foreland basin supports the hypothesis of Cina et al. (2009) that the Yalu River may have been captured at times by transverse rivers across the Himalayan crest.

DISCUSSION

Our work on the nature of river detritus from the Yalu River system integrates several approaches, including the U-Pb dating and Hf isotope analysis of detrital zircon, analysis of river sand composition, and statistic comparison of age spectra of zircon from the source regions, delivery systems, and sinks. The main results of our work may be summarized as follows.

(1) In a ZA-ZH plot, we find that zircon populations of bedrock (sedimentary, plutonic, and volcanic) in the Lhasa River drainage basin,
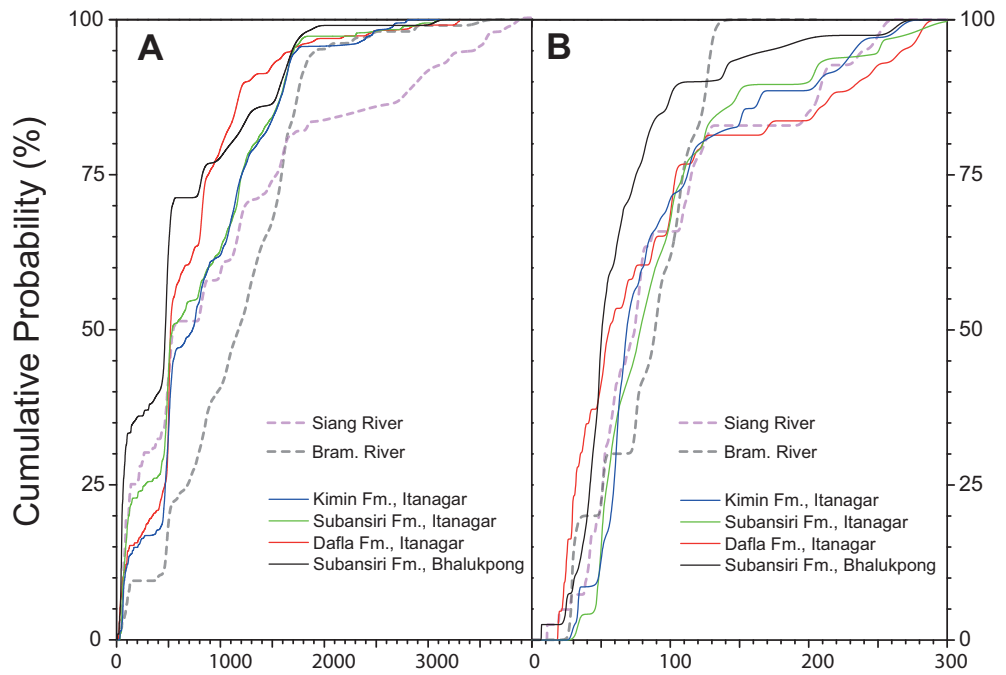
Figure 9. Cumulative probability plots of detrital-zircon ages of modern river sand from the Siang and Brahmaputra Rivers and Neogene sandstone samples from the eastern Himalayan foreland at the range of 0–4000 Ma (A) and the range of 0–300 Ma (B). The detailed relative probability plots of four Neogene sandstone samples from Cina et al. (2009) are shown in C, D, E, and F.
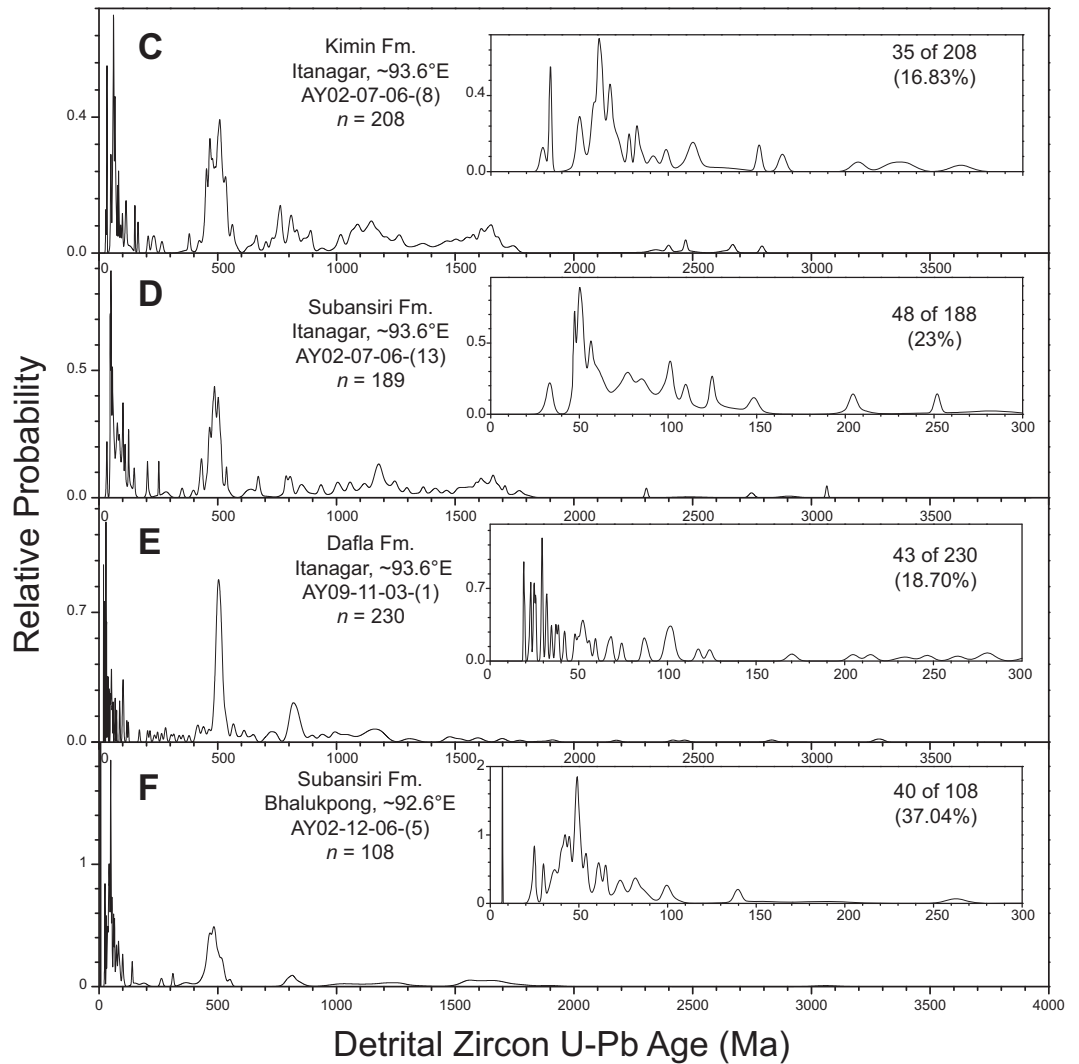
the largest tributary of the Yalu River, are significantly different from zircon populations of the Lhasa River sand (Figs. 7B–7E).

(2) The short tributaries north of the Yalu River display dominant U-Pb zircon ages clustered at 50 Ma to 65 Ma (Fig. 3). In contrast, all samples from the long tributaries north of the Yalu River except that from the Nyingoh River display a prominent age peak at 110–120 Ma, which is absent for samples from the short tributaries (Fig. 3).

(3) Although the long rivers carry the 110–120 Ma age clusters and mostly negative Hf isotopic signatures of the northern Lhasa terrane, the Yalu River samples in general do not display them (Figs. 4C and 5C; cf. Figs. 2A and 2F). Instead, the main trunk of the Yalu River is dominated by the 50 Ma age peak, the characteristic age of the southern Gangdese zone. Only samples collected from the segments of the Yalu River that lie entirely in the Himalayan orogen (i.e., sites at the Saga, Siang River, and Brahmaputra River) display 500 Ma age peaks (Fig. 4).

(4) For Hf isotope analysis, samples from the short and long tributaries north of the Yalu River display a wide range of $\varepsilon_{Hf}(t)$ isotopic values from –15 to +15. However, the main trunk of the Yalu River preferentially records the $\varepsilon_{Hf}(t)$ signals from the southern Gangdese zone.

(5) Except where the Yalu River flows over the Himalayan orogen (i.e., the Saga sample), the proportion of 0–300 Ma detrital zircons exceeds 50% for the samples collected from the Yalu River (i.e., the Quxu, Gonggar, and Gyaca samples), but this proportion drops to 26% for the Siang River sample and to only 10% in the Brahmaputra River sample (Fig. 4).

(6) The age spectra of some late Cenozoic samples from the eastern Himalayan foreland are more similar to the age spectra of the Yalu River samples located north of the Himalayan crest rather than those of the Siang and Brahmaputra River samples located south of the Himalayan crest.

(7) There are appreciable differences between the age spectra of bedrock zircon and those of river sand samples (e.g., the Renbu Qu and Siqunama River samples contain zircon grains that better match the Lhasa terrane zircon population than the known bedrock ages of the Himalayan orogen despite the fact that the two streams flow across the Himalaya).

(8) Except for the Zedong tributary sample, the proportion of lithic fragments from short rivers (L = 23%–28%) is significantly less than that of the long rivers (L = 37%–48%) (Table 2). The proportion of lithic fragments also increases downstream along the Yalu River, from ~40% to ~60% over a distance of ~700 km (Table 2; see Fig. 1B for sample locations).

(9) The Renbu Qu, draining only the Himalayan orogens, contains 50 Ma zircon grains that are apparently derived from the Lhasa terrane north.

These observations and research results have important implications for the evolution of the Yalu River system. Next, we discuss two issues in light of our newly obtained results: (1) the role of transport distance and climate conditions in controlling sediment load in the Yalu River, and (2) the implications of the age spectra of the Yalu-Siang-Brahmaputra samples for reconstructing the evolution of the Himalayan drainage system.

Downstream Dilution of Detrital-Zircon Age Signals

Cina et al. (2009) noted that the proportion of 0–200 Ma zircon derived from the Lhasa terrane decreases dramatically across the eastern Himalayan syntaxis, from ~70% along the Yalu River to less than 10% along the Brahmaputra River. They attributed this observation to a dilution effect by the exceedingly high erosion rates across the eastern Himalayan syntaxis. The same conclusion was also reached by Garzanti et al. (2004), Stewart et al. (2008), and Finnegan et al. (2008). This process is shown schematically in Figure 10, in which the composition of detrital zircon evolves with time due to progressive addition of new zircon populations from downstream banks and tributaries. This simple evolution diagram assumes that each new source area on the left bank of the main stream contributes to 25% of the total number of detrital zircon while the homogeneous source area on the right bank of the river provides constant detrital supply at 50%. In this case, the proportion of zircon from source domains 1a and 1b decreases progressively, and the smaller component (1a) eventually becomes undetectable (i.e., at stage E in Fig. 10). For the case of the Yalu River, we think that this dilution effect is more prominent. This is because the inferred erosion rates based on topographic and precipitation data increase eastward across the Yalu River basin (Finlayson et al., 2002). This means that more detritus is produced per area downstream along the Yalu River. It should also be noted that the production rate of detritus increases dramatically at the Yarlung gorge as the Yalu River crosses the eastern Himalayan syntaxis (Finnegan et al., 2008), further enhancing the dilution effect.

Cina et al.'s (2009) proposal was based on the age spectrum of one sample from the Yalu River (i.e., Gonggar sample AY06–28–06-[1] at site c in Fig. 1B) (Table 1). Our additional sampling of modern sand from the Yalu River confirms this general suggestion, but with a caveat. The Quxu

and Gyaca samples were collected along a segment of the Yalu River that follows the trace of the Indus-Tsangpo suture zone. The age spectra of these samples indicate a high proportion of Lhasa terrane detrital zircon at 56% and 59% for an age range of 0–300 Ma (Fig. 4). In contrast, the age spectrum of the Saga sample, which was collected along a segment of the Yalu River that flows within the Himalayan orogen, only yields 24% of zircon in the age range of 0–300 Ma (Fig. 4). This means that the composition of detrital zircon in the Yalu River sand is highly sensitive to the course of the river. Downstream dilution of zircon age signals is also seen in tributaries of the Yalu River.

Topography, Climate, and Spatially Varying Stream Power

Although it is not the main focus of this study and our sampling coverage is highly incomplete, the analysis of sandstone modal composition based on three samples at Saga, Quxu, and Gyaca sites from the Yalu River indicates a marked increase in the proportion of lithic fragments downstream (Table 2; see Fig. 1B for sample locations). There are two main factors that favor high production of lithic fragments in river sand: (1) the presence of source rocks that are easily broken down and (2) a downstream increase in stream power induced by higher topographic relief and strong precipitation. Both processes could have shortened the delivery time from the source to the main stream and thus enhance the chance of preserving lithic fragments (e.g., Johnson, 1993; Cox and Lowe, 1995; Le Pera et al., 2001; Le Pera and Arribas, 2004; Garzanti et al., 2004; Finnegan et al., 2008). We consider that the lithologic control of the source rock is not a main controlling factor for the observed increase in lithic fragments. This is because the downstream increase in the proportion of lithic fragments does not depend on the exact course of the Yalu River, which traverses both the Himalayan orogen and along the Indus-Tsangpo suture. In addition, there is no systematic variation in lithology of the Lhasa terrane and the Himalayan orogen along the Yalu River despite some local changes (Pan et al., 2004). In contrast, there is a systematic change in the climatic condition along the strike of the Himalayan Range; that is, the duration and intensity of precipitation increase eastward due to the effect of the Indian summer monsoon (Finlayson et al., 2002; Bookhagen and Burbank, 2006). This effect would lead to an eastward increase in discharge and thus stream power (Finlayson et al., 2002) and a reduction of the residence time of detritus in the fluvial delivery systems. The relief of the Yalu River

Dilution of zircon-age populations of upper-stream due to progressive addition of new detritus from main stream boundary domains
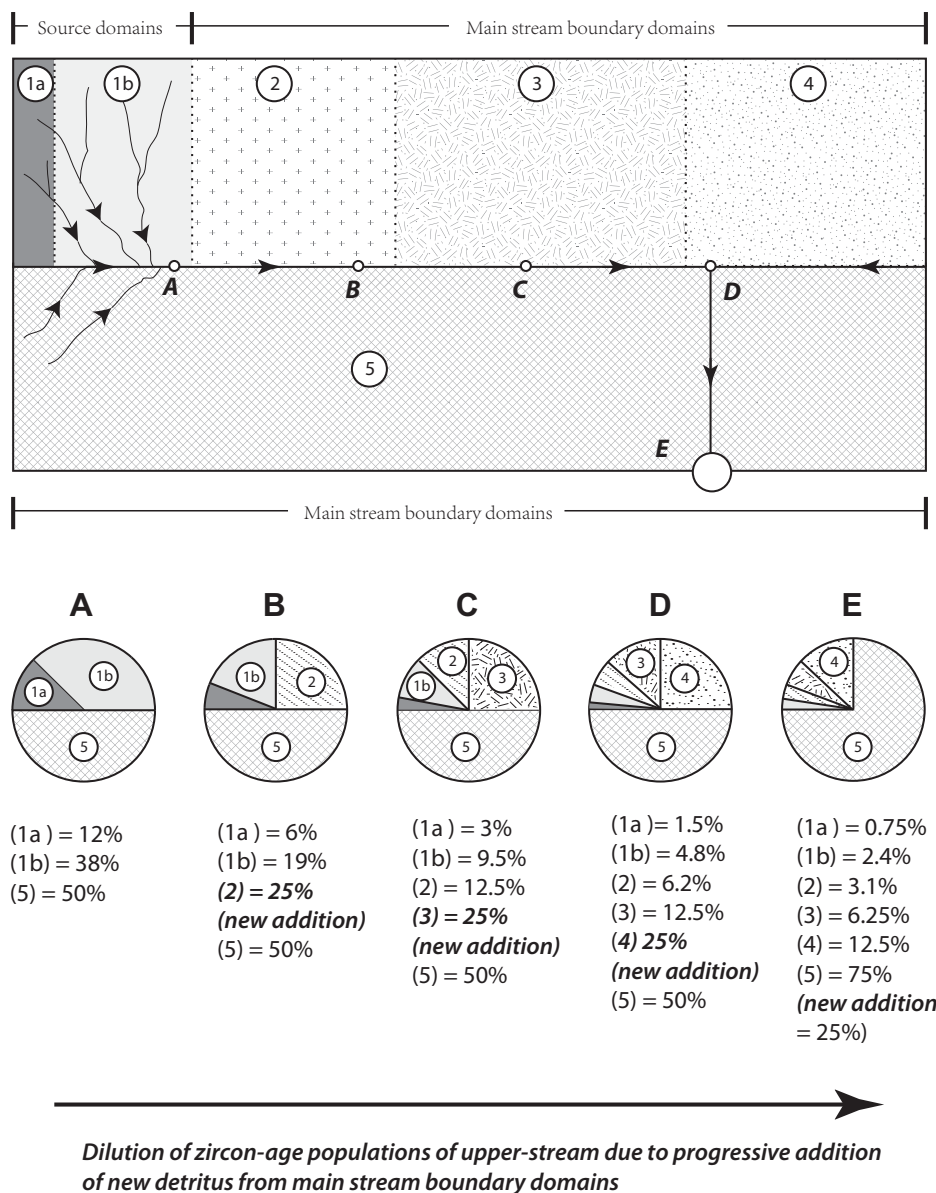
Figure 10. Systematic downstream dilution of zircon populations as a result of addition of new provenance components. Numbers 1a, 1b, 2, 3, 4, and 5 represent hypothetically distinctive provenance domains, while A, B, C, D, and E are hypothetical sample sites. The dilution process makes the simple assumptions that each newly emerged source area on the left bank contributes to 25% of the total zircon volume in the river sand while the contribution from source region 5 maintains a constant level of 50% when the mainstream runs along its edge bordering other domains.

Valley and its drainage basin also increases markedly from west to east, particularly east of 90°E (Fig. 1A), which may further shorten the residence time of detritus in the delivery systems, leading to an eastward increase in the lithic fragments in the river sand.

An important issue that is not discussed is the discharge of Yalu tributaries and their relative magnitude between each other and against that of the Yalu River at its various segments.

This may be achieved by the use of an isohyets map (i.e., a map showing contours of rainfall distribution) across the Yalu Basin. Knowledge concerning the spatial distribution of tributary discharges and the spatial distribution of bedrock zircon-population distributions will provide better information for quantifying how zircon populations from the source regions are linked to zircon populations in the main trunk of the Yalu River.

Late Cenozoic Evolution of the Himalayan Drainage System

Burrard and Hayden (1907) divided the Himalayan drainages into the longitudinal (e.g., the Yalu and Indus Rivers) and transverse rivers (e.g., the Teesta, Subansiri, and Sutlej Rivers) that flow parallel to and across the orogen (Fig. 1). Four models have been proposed for the origin of the longitudinal rivers, which we briefly discuss here in order to highlight the different predictions in the composition of detrital zircon (Fig. 1C). Many Himalayan rivers are considered antecedent to the uplift of the Himalayan Range (Medlicott, 1868; Burrard and Hayden, 1907; Hayden, 1907; Heron, 1922; Wager, 1937). Brookfield (1998, p. 294) was the first to place this idea in the context of a deforming Asian continent. He pointed out the potential utilities of large rivers as Cenozoic strain markers following the early suggestion of Tapponnier et al. (1986). Hallet and Molnar (2001) interpreted the anomalous spacing of large rivers in southeast Tibet as a product of >1000 km of right-slip shear. Both Brookfield (1998) and Hallet and Molnar (2001) considered that major rivers in the Himalayan-Tibetan orogen have been fixed in the deforming Asian crust over tens of millions of years. This implies that the provenance domains bordering the Yalu River have been maintained since the initial uplift of the Himalaya, although their shape may have changed with time. This antecedent model predicts that only the Brahmaputra River is capable of delivering the detritus of all five provenance domains described in Figure 1C to the eastern Himalayan foreland (Fig. 11A).

In contrast to a constant configuration of the Yalu River, Seeber and Gornitz (1983) suggested that the Yalu River was once linked with the Lohit River before it was captured by the Siang River. Alternatively, Brookfield (1998) considered the Yalu was linked with the Irrawaddy River and was not captured by the Siang-Brahmaputra River until ca. 10 Ma (Fig. 11B). Zeitler et al. (2001) and Clark et al. (2004) supported this hypothesis but considered a younger capture time in the past few million years. This hypothesis implies that the eastern Himalayan foreland basin was disconnected with the Lhasa terrane source rocks until 10 Ma or more recently.

Hayden (1907) and Heron (1922) suggested that some south-flowing Himalayan transverse rivers may have periodically captured the longitudinal Yalu and Indus Rivers induced by their energetically favored headward erosion. This idea was expanded by Cina et al. (2009), who showed that the presence of 0–200 Ma detrital zircon could have been delivered by a transverse

Figure 11. The competing models for the origin and evolution of the Yalu-Brahmaputra River system. (A) The antecedent river hypothesis; (B) the ancestral Yalu-Irrawaddy hypothesis (before 10–4 Ma); (C) the short-cut transverse river hypothesis; and (D) the multiple-dam hypothesis.

river such as the Subansiri River in the eastern Himalaya in the Pliocene (Fig. 11C).

A more general case is that the Yalu was periodically diverted into a transverse river across the central segment of the Himalaya, possibly induced by intermittent formation of high dams that blocked the eastward flow of the Yalu River through the eastern syntaxis (Fig. 11D). Several narrow gorges along the Yalu River and their proximity to active north-trending rifts (e.g., Zhang, 1998, 2001) would have been ideal places to initiate large landslides to temporarily block the Yalu River. Periodic advances of glaciers forming ice dams and large lakes behind them have also been shown to have occurred along the Yalu River in the Quaternary (Zhang, 1998; Montgomery et al., 2004). Thus, local connection between the Yalu River and one of the major Himalayan transverse rivers may have led to local flow reversal of the Yalu main stream and a direct delivery of detritus from the Lhasa terrane to the Himalayan foreland.

The models for the past Yalu-Lohit and Yalu-Irrawaddy connections may be tested by examining the detrital-zircon signatures in the foreland basin sediments of the eastern Himalaya in light of our new data as a basis for comparisons. However, our modern sand data alone cannot test these models. What we can test is whether the Neogene foreland sediments were derived from the past Brahmaputra River, if it had exactly the same geometry and sand composition as it has today. Quantitative comparisons of detrital-zircon age spectra and the corresponding $\varepsilon_{Hf}(t)$ values between Neogene foreland sediments and modern river sand of the Yalu River (Table 3; Figs. 4, 5, and 9) suggest that the Dafla sample from Itanagar (site H-2 in Fig. 1B) is more similar to all those of the Yalu River samples than the Siang and Brahmaputra samples for the age range of 0–300 Ma. Furthermore, its corresponding $\varepsilon_{Hf}(t)$ values closely resemble those of the Gonggar and Gyaca samples. The overlying Subansiri and Kimin samples are very different from the Dafla sample and are indistinguishable from the sample from the Siang River. This is especially the case for their age spectra in the range of 0–300 Ma and the relevant $\varepsilon_{Hf}(t)$ values. The age spectrum of the Subansiri sample collected at the Bhalukpong site (H-1 site in

Zhang et al.
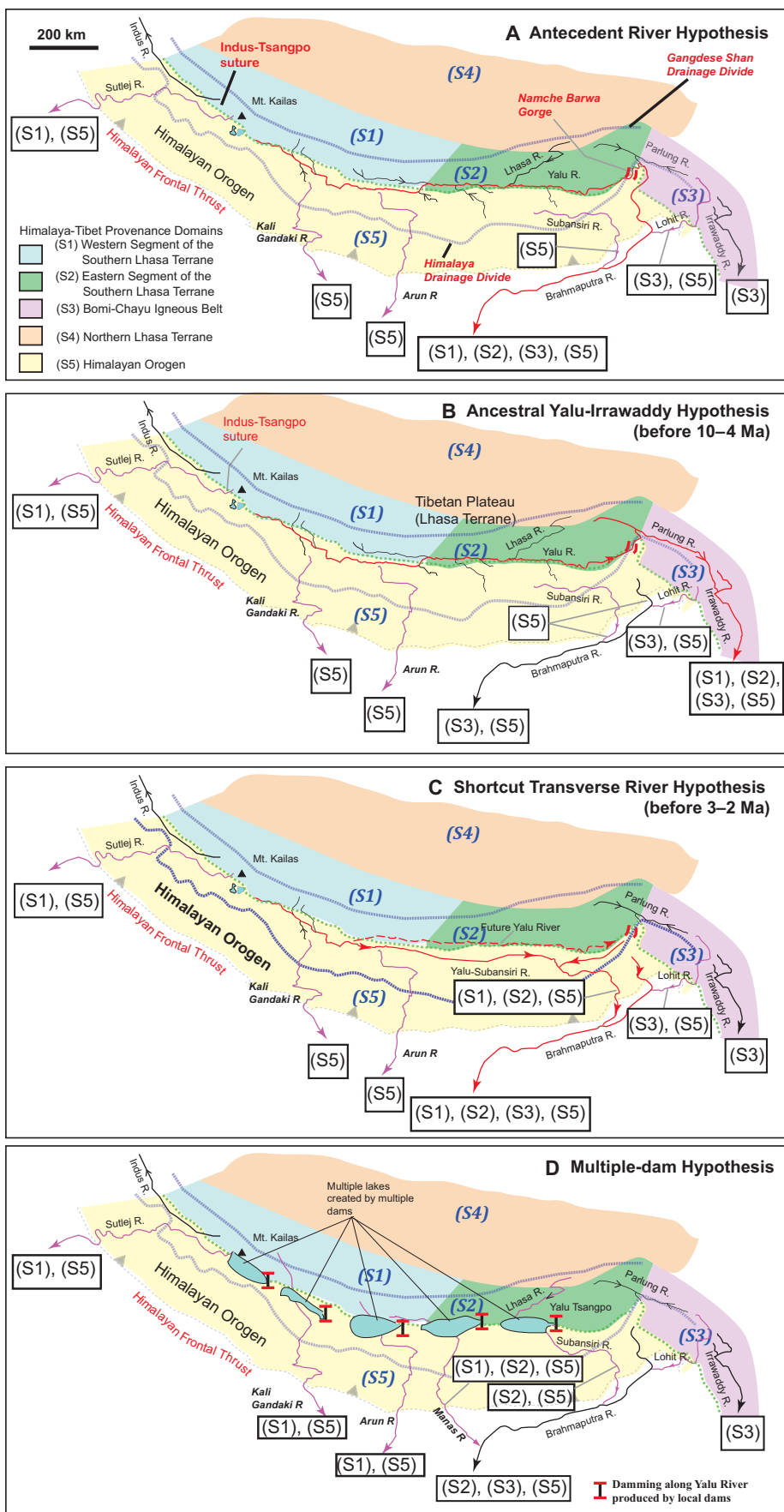
Fig. 1B) is more similar to those of the Gonggar and Gyaca samples than those of the Siang and Brahmaputra samples. If the along-river distribution of zircon populations in the Yalu, Siang, and Brahmaputra Rivers has stayed the same since the late Miocene and early Pliocene, when the Dafla and Subansiri strata were deposited, the results of these comparisons imply that the Himalayan foreland sediments had differing provenance from that of the Siang-Brahmaputra and Yalu Rivers. The simplest explanation for this is that the river flowed directly across the eastern Himalaya without going through the eastern syntaxis. Sediments of the late Miocene Dafla Formation and Pliocene Subansiri Formation were probably delivered through transient crossings of the Himalaya by the Yalu River via its connection with Himalayan transverse rivers such as the Subansiri River. We suggest that the Yalu River has taken the alternative modes of the antecedent-river and shortcut-river courses to deliver detritus to the eastern Himalayan foreland basin in the past 10–5 m.y. These inferences require that the erosional rates of the Yalu-Siang-Brahmaputra drainage basin have not varied with time in the past 10–5 m.y. This contradicts the observation from the eastern Himalayan syntaxis, where the exhumation rate has accelerated in the past 5 m.y. (e.g., Finnegan et al., 2008, and references therein). However, this acceleration would have delivered more Siang River zircon populations into the Himalayan foreland basin, for which there is no such evidence.

Sand Transport: Fluvial or Eolian Processes

A 160 Ma single zircon was detected from the Siqunama River sample draining the Himalayan orogen (Fig. 3J; also see sample site 10 in Fig. 1B for location). This age is unknown from the Himalayan bedrock but prevalent in the Gangdese batholith of the Lhasa terrane. The 160 Ma grain could have been derived from an unrecognized source storing Gangdese zircons in the Himalayan orogen (e.g., abandoned river terraces). It is also possible that the grain was transported by wind from the northern Lhasa terrane or even the Qiangtang terranes in central Tibet, where igneous rocks of such age are common (e.g., Yin and Harrison, 2000; Pan et al., 2004). Similar explanations may also apply to the Renbu Qu sample that contains two 50 Ma zircon grains, characteristic to the southern Gangdese igneous zone (Fig. 3I). The presence of many dry lakes and lake shorelines exposing beach sand across a vast area of central Tibet (e.g., Avouac et al., 1996; Owen et al., 2006) may serve as the sources of some of the detrital

grains seen in the Lhasa River sample. Since most conventional detrital-zircon provenance analyses assume fluvial transport linking the source rocks to the related sedimentary basins (cf. Pullen et al., 2011), it is important to further test this possibility by dating cobbles of igneous rocks in river sand. When the proportion of the "unexplainable" zircon grains is extremely small (1 or 2 grains out of ~100 grains), the eolian process as a delivery mechanism of detrital zircon, if it occurred at all across the Yalu River basin, must be much less important than the fluvial delivery processes. Besides eolian transport, the mismatch in age spectra between river sand and bedrock may be explained by lack of systematic dating of bedrock, erosional removal or burial of the source rocks in recent times (e.g., Wu et al., 2010), and exposure area and detrital production rates of individual rock units containing particular zircon populations.

CONCLUSIONS

The characterization of ages and Hf isotopes of zircon populations along different segments of the Yalu River and its tributaries led to the following inferences. First, the presence or absence of distinctive zircon populations in the main stream of the Yalu River depends strongly on the configuration of its tributaries. The correlation of zircon populations between those from the source rocks and those preserved in river sand also depends on the burial and exhumation history of the source rocks and possible mixing of a minor amount of detritus from outside the drainage basin through eolian processes. Second, the proportion of zircon populations in the Yalu River sand decreases systematically downstream, caused by the dilution effects; in some extreme cases, the upstream signals can completely be lost. Third, a downstream increase in lithic fragments along the Yalu River may be attributed to an eastward increase in the topographic relief and annual precipitation. Fourth, similarities in zircon populations between the Yalu River sand and Neogene foreland sediments support the proposal that the Yalu River had once flowed through the Himalaya significantly (hundreds of kilometers) west of its current course across the mountain range at the eastern syntaxis. This shortcut process appears to have been transient, recorded only in specific stratigraphic horizons of foreland sediments. Diversion of the Yalu River into the foreland basin without going through the eastern syntaxis may have been caused by glacier advances or emplacements of large landslides that temporarily dammed the Yalu River. Alternatively, the lack of eastern syntaxis zircon populations in foreland sediments of the eastern Himalaya

may have been caused by its low erosion rate at the time of foreland sedimentation, leading to the dominant appearance of upper-stream zircon populations from the Yalu River in foreland sediments.

REFERENCES CITED

Aikman, A.B., Harrison, T.M., and Ding, L., 2008, Evidence for early (>44 Ma) Himalayan crustal thickening, Tethyan Himalaya, southeastern Tibet: Earth and Planetary Science Letters, v. 274, p. 14–23, doi:10.1016/j.epsl.2008.06.038.

Amidon, W.H., Burbank, D.W., and Gehrels, G.E., 2005, Construction of detrital mineral populations: Insights from mixing of U-Pb zircon ages in Himalayan rivers: Basin Research, v. 17, p. 463–485, doi:10.1111/j.1365-2117.2005.00279.x.

Andersen, T., 2002, Correction of common lead in U-Pb analyses that do not report [204]Pb: Chemical Geology, v. 192, p. 59–79, doi:10.1016/S0009-2541(02)00195-X.

Avouac, J.P., Dobremez, J.F., and Bourjot, L., 1996, Palaeoclimatic interpretation of a topographic profile across middle Holocene regressive shorelines of Longmu Co (western Tibet): Palaeogeography, Palaeoclimatology, Palaeoecology, v. 120, p. 93–104, doi:10.1016/0031-0182(96)88700-1.

Bookhagen, B., and Burbank, D.W., 2006, Topography, relief, and TRMM-derived rainfall variations along the Himalaya: Geophysical Research Letters, v. 33, p. L08405, doi:10.1029/2006GL026037.

Brookfield, M.E., 1998, The evolution of the great river systems of southern Asia during the Cenozoic India-Asia collision: Rivers draining southwards: Geomorphology, v. 22, p. 285–312, doi:10.1016/S0169-555X(97)00082-2.

Burchfiel, B.C., Chen, Z., Hodges, K.V., Liu, Y., Royden, L.H., Deng, C., and Xu, J., 1992, The South Tibetan detachment system, Himalayan orogen: Extension contemporaneous with and parallel to shortening in a collisional mountain belt: Geological Society of America Special Paper 269, 41 p.

Burrard, S.G., and Hayden, H.H., 1907, A Sketch of the Geography and Geology of the Himalaya Mountains and Tibet: Calcutta, India, Superintendent Government Printing, 308 p.

Cai, F.L., Ding, L., and Yue, Y.Y., 2011, Provenance analysis of Upper Cretaceous strata in the Tethys Himalaya, southern Tibet: Implications for timing of India-Asia collision: Earth and Planetary Science Letters, v. 305, p. 195–206, doi:10.1016/j.epsl.2011.02.055.

Che, J., Zhou, W.W., Hu, J.S., Yan, F., Papenfuss, T.J., Wake, D.B., and Zhang, Y.P., 2010, Spiny frogs (Paini) illuminate the history of the Himalayan region and Southeast Asia: Proceedings of the National Academy of Sciences of the United States of America, v. 107, p. 13,765–13,770, doi:10.1073/pnas.1008415107.

Chiu, H.Y., Chung, S.L., Wu, F.Y., Liu, D., Liang, Y.H., and Lin, I., 2009, Zircon U-Pb and Hf isotopic constraints from eastern Transhimalayan batholiths on the precollisional magmatic and tectonic evolution in southern Tibet: Tectonophysics, v. 477, p. 3–19, doi:10.1016/j.tecto.2009.02.034.

Chu, M.F., Chung, S.L., Song, B., Liu, D.Y., O'Reilly, S.Y., Pearson, N.J., Ji, J.Q., and Wen, D.J., 2006, Zircon U-Pb and Hf isotope constraints on the Mesozoic tectonics and crustal evolution of southern Tibet: Geology, v. 34, p. 745–748, doi:10.1130/G22725.1.

Chung, S.L., Chu, M.F., Ji, J.Q., O'Reilly, S.Y., Pearson, N.J., Liu, D.Y., Lee, T.Y., and Lo, C.H., 2009, The nature and timing of crustal thickening in southern Tibet: Geochemical and zircon Hf isotopic constraints from postcollisional adakites: Tectonophysics, v. 477, p. 36–48, doi:10.1016/j.tecto.2009.08.008.

Cina, S., Yin, A., Grove, M., Dubey, C.S., Shukla, D.P., Lovera, O.M., Kelty, T.K., Gehrels, G.E., and Foster, D.A., 2009, Gangdese arc detritus within the eastern Himalayan Neogene foreland basin: Implications for the Neogene evolution of the Yalu-Brahmaputra River system: Earth and Planetary Science Letters, v. 285, p. 150–162, doi:10.1016/j.epsl.2009.06.005.

Clark, M.K., Schoenbohm, L.M., Royden, L.H., Whipple, K.X., Burchfiel, B.C., Zhang, X., Tang, W., Wang, E., and Chen, L., 2004, Surface uplift, tectonics, and erosion of eastern Tibet from large-scale drainage patterns: Tectonics, v. 23, p. 1006–1029, doi:10.1029/2002TC001402.

Clark, M.K., Royden, L.H., Whipple, K.X., Burchfiel, B.C., Zhang, X., and Tang, W., 2006, Use of a regional, relict landscape to measure vertical deformation of the eastern Tibetan Plateau: Journal of Geophysical Research, v. 111, p. F03002, doi:10.1029/2005JF000294.

Clift, P.D., 2006, Controls on the erosion of Cenozoic Asia and the flux of clastic sediment to the ocean: Earth and Planetary Science Letters, v. 241, p. 571–580, doi:10.1016/j.epsl.2005.11.028.

Clift, P.D., Long, H.V., Hinton, R., Ellam, R.M., Hannigan, R., Tan, M.T., Blusztajn, J., and Duc, N.A., 2008a, Evolving East Asian river systems reconstructed by trace element and Pb and Nd isotope variations in modern and ancient Red River–Song Hong sediments: Geochemistry, Geophysics, Geosystems, v. 9, p. Q04039, doi:10.1029/2007GC001867.

Clift, P.D., Hodges, K.V., Heslop, D., Hannigan, R., Long, H.V., and Calves, G., 2008b, Correlation of Himalayan exhumation rates and Asian monsoon intensity: Nature Geoscience, v. 1, p. 875–880, doi:10.1038/ngeo351.

Cox, R., and Lowe, D.R., 1995, A conceptual review of regional-scale controls on the composition of clastic sediment and the co-evolution of continental blocks and their sedimentary cover: Journal of Sedimentary Research, v. 65, p. 1–12.

DeCelles, P.G., Gehrels, G.E., Quade, J., LaReau, B., and Spurlin, M., 2000, Tectonic implications of U-Pb zircon ages of the Himalayan orogenic belt in Nepal: Science, v. 288, p. 497–499, doi:10.1126/science.288.5465.497.

DeCelles, P.G., Gehrels, G.E., Najman, Y., Martin, A.J., Carter, A., and Garzanti, E., 2004, Detrital geochronology and geochemistry of Cretaceous–early Miocene strata of Nepal: Implications for timing and diachroneity of initial Himalayan orogenesis: Earth and Planetary Science Letters, v. 227, p. 313–330, doi:10.1016/j.epsl.2004.08.019.

Dickinson, W.R., 1970, Interpreting detrital modes of greywacke and arkose: Journal of Sedimentary Research, v. 40, p. 695–707.

Dickinson, W.R., 1985, Interpreting provenance relations from detrital modes of sandstones, *in* Zuffa, G.G., ed., Provenance of arenites: NATO ASI Series C: 148: Dordrecht/Boston/Lancaster, D. Reidel Publishing Company, p. 333–361.

Ding, L., Zhong, D.L., Yin, A., Kapp, P., and Harrison, T.M., 2001, Cenozoic structural and metamorphic evolution of the eastern Himalayan syntaxis (Namche Barwa): Earth and Planetary Science Letters, v. 192, p. 423–438, doi:10.1016/S0012-821X(01)00463-0.

Dodson, M.H., Compston, W., Williams, I.S., and Wilson, J.F., 1988, A search for ancient detrital zircons in Zimbabwean sediments: Journal of the Geological Society of London, v. 145, p. 977–983, doi:10.1144/gsjgs.145.6.0977.

Dürr, S.B., 1996, Provenance of Xigaze fore-arc basin clastic rocks (Cretaceous, south Tibet): Geological Society of America Bulletin, v. 108, p. 669–684, doi:10.1130/0016-7606(1996)108<0669:POXFAB>2.3.CO;2.

Enkelmann, E., Ehlers, T.A., Zeiler, P.K., and Hallet, B., 2011, Denudation of the Namche Barwa antiform, eastern Himalaya: Earth and Planetary Science Letters, v. 307, p. 323–333, doi:10.1016/j.epsl.2011.05.004.

Finlayson, D.P., Montgomery, D.R., and Hallet, B., 2002, Spatial coincidence of rapid inferred erosion with young metamorphic massifs in the Himalayas: Geology, v. 30, p. 219–222, doi:10.1130/0091-7613(2002)030<0219:SCORIE>2.0.CO;2.

Finnegan, N.J., Hallet, B., Montgomery, D.R., Zeitler, P.K., Stone, J.O., Anders, A.M., and Liu, Y.P., 2008, Coupling of rock uplift and river incision in the Namche Barwa–Gyala Peri massif, Tibet: Geological Society of America Bulletin, v. 120, p. 142–155, doi:10.1130/B26224.1.

Gansser, A., 1964, The Geology of the Himalayas: New York, Wiley Interscience, 289 p.

Garzanti, E., Vezzoli, G., Ando, S., France-Lanord, C., Singh, S.K., and Foster, G., 2004, Sand petrology and focused erosion in collision orogens: The Brahmaputra case: Earth and Planetary Science Letters, v. 220, p. 157–174, doi:10.1016/S0012-821X(04)00035-4.

Gazzi, P., 1966, Le arenarie del flysch sopracretaceo dell'Appennino modenese; correlazioni con il flysch di Monghidoro: Acta Mineralogica-Petrographica, v. 12, p. 69–97.

Gehrels, G.E., Yin, A., and Wang, X.F., 2003, Detrital-zircon geochronology of the northeastern Tibetan Plateau: Geological Society of America Bulletin, v. 115, p. 881–896, doi:10.1130/0016-7606(2003)115<0881:DGOTNT>2.0.CO;2.

Gehrels, G., Kapp, P., DeCelles, P., Pullen, A., Blakey, R., Weislogel, A., Ding, L., Guynn, J., Martin, A., McQuarrie, N., and Yin, A., 2011, Detrital zircon geochronology of pre-Tertiary strata in the Tibetan-Himalayan orogen: Tectonics, v. 30, p. TC5016, doi:10.1029/2011TC002868.

Grujic, D., Coutand, I., Bookhagen, B., Bonnet, S., Blythe, A., and Duncan, C., 2006, Climatic forcing of erosion, landscape, and tectonics in the Bhutan Himalayas: Geology, v. 34, p. 801–804, doi:10.1130/G22648.1.

Guynn, J.H., Kapp, K., Pullen, A., Heizler, M., Gehrels, G., and Ding, L., 2006, Tibetan basement rocks near Amdo reveal "missing" Mesozoic tectonism along the Bangong suture, central Tibet: Geology, v. 34, p. 505–508, doi:10.1130/G22453.1.

Hallet, B., and Molnar, P., 2001, Distorted drainage basins as markers of crustal strain east of the Himalaya: Journal of Geophysical Research, v. 106, p. 13,697–13,709, doi:10.1029/2000JB900335.

Harris, N.B.W., Xu, R.H., Lewis, C.L., Hawkeworth, C.J., and Zhang, Y.Q., 1988, Isotope geochemistry of the 1985 Tibet Geotraverse, Lhasa to Golmud: Royal Society of London Philosophical Transactions, ser. A, v. 327, p. 263–285, doi:10.1098/rsta.1988.0129.

Harris, N.B.W., Inger, S., and Xu, R.H., 1990, Cretaceous plutonism in Central Tibet: An example of post-collision magmatism: Journal of Volcanology and Geothermal Research, v. 44, p. 21–32, doi:10.1016/0377-0273(90)90009-5.

Harrison, T.M., Grove, M., Lovera, O.M., and Catlos, E.J., 1998, A model for the origin of Himalayan anatexis and inverted metamorphism: Journal of Geophysical Research, v. 103, p. 27,017–27,032, doi:10.1029/98JB02468.

Harrison, T.M., Yin, A., Grove, M., Lovera, O.M., Ryerson, F.J., and Zhou, X., 2000, The Zedong Window: A record of superposed Tertiary convergence in southeastern Tibet: Journal of Geophysical Research, v. 105, p. 19,211–19,230, doi:10.1029/2000JB900078.

Hayden, M.M., 1907, The geology of the provinces of Tsang and Ü in central Tibet: Memoirs of the Geological Survey of India, v. 36, p. 122–201.

He, S.D., Kapp, P., DeCelles, P.G., Gehrels, G.E., and Heizler, M., 2007, Cretaceous–Tertiary geology of the Gangdese arc in the Linzhou area, southern Tibet: Tectonophysics, v. 433, p. 15–37, doi:10.1016/j.tecto.2007.01.005.

Heron, A.M., 1922, Geological results of the Mt. Everest reconnaissance expedition: Memoirs of the Geological Survey of India, v. 54, p. 215–234.

Hoorn, C., Wesselingh, F.P., ter Steege, H., Bermudez, M.A., Mora, A., Sevink, J., Sanmartín, I., Sanchez-Meseguer, A., Anderson, C.L., Figueiredo, J.P., Jaramillo, C., Riff, D., Negri, F.R., Hooghiemstra, H., Lundberg, J., Stadler, T., Särkinen, T., and Antonelli, A., 2010, Amazonia through time: Andean uplift, climate change, landscape evolution, and biodiversity: Science, v. 330, p. 927–931, doi:10.1126/science.1194585.

Hu, D.G., Wu, Z.H., Wan, J., Shi, Y.R., Ye, P.S., and Liu, Q.S., 2005, SHRIMP zircon U-Pb age and Nd isotopic study on the Nyainqentanglha Group in Tibet: Science in China Series D–Earth Sciences, v. 48, p. 1377–1386.

Hu, X.M., Jansa, L., Chen, L., Griffin, W.L., O'Reilly, S.Y., and Wang, J.G., 2010, Provenance of Lower Cretaceous Wölong volcaniclastics in the Tibetan Tethyan Himalaya: Implications for the final breakup of Eastern Gondwana: Sedimentary Geology, v. 223, p. 193–205, doi:10.1016/j.sedgeo.2009.11.008.

Iizuka, T., Hirata, T., Komiya, T., Rino, S., Katayama, I., Motoki, A., and Maruyama, S., 2005, U-Pb and Lu-Hf isotope systematics of zircons from the Mississippi River sand: Implications for reworking and growth of continental crust: Geology, v. 33, p. 485–488, doi:10.1130/G21427.1.

Ingersoll, R.V., Bullard, T.P., Ford, R.L., Grimm, P., Pickle, L.D., and Sares, S.W., 1984, The effect of grain size on detrital modes: A test of the Gazzi-Dickinson point-counting method: Sedimentary Petrology, v. 54, p. 103–116.

Ji, W.Q., 2010, Geochronology and Petrogenesis of Granitic Rocks from East Segment of the Gangdese Batholith, Southern Tibet [Ph.D. thesis]: Beijing, Institute of Geology and Geophysics, Chinese Academy, p. 1–134 (in Chinese with English abstract).

Ji, W.Q., Wu, F.Y., Chung, S.L., Li, J.X., and Liu, C.Z., 2009, Zircon U-Pb geochronology and Hf isotopic constraints on petrogenesis of the Gangdese batholith, southern Tibet: Chemical Geology, v. 262, p. 229–245, doi:10.1016/j.chemgeo.2009.01.020.

Johnson, M.J., 1993, The system controlling the composition of clastic sediments, *in* Johnson, M.J., and Basu, A., eds., Processes Controlling the Composition of Clastic Sediments: Geological Society of America Special Paper 284, p. 147–157.

Kapp, J.L., Harrison, T.M., Kapp, P., Grove, M., Lovera, O.M., and Ding, L., 2005, Nyainqentanglha Shan: A window into the tectonic, thermal, and geochemical evolution of the Lhasa block, southern Tibet: Journal of Geophysical Research, v. 110, p. B08413, doi:10.1029/2004JB003330.

Kapp, P., DeCelles, P.G., Gehrels, G.E., Heizler, M., and Ding, L., 2007a, Geological records of the Lhasa-Qiangtang and Indo-Asian collisions in the Nima area of central Tibet: Geological Society of America Bulletin, v. 119, p. 917–933, doi:10.1130/B26033.1.

Kapp, P., DeCelles, P.G., Leier, A.L., Fabijanic, J.M., He, S., Pullen, A., and Gehrels, G.E., 2007b, The Gangdese retroarc thrust belt revealed: GSA Today, v. 17, no. 7, p. 4–9, doi:10.1130/GSAT01707A.1.

King, J., Harris, N., Argles, T., Parrish, R., and Zhang, H.F., 2011, Contribution of crustal anatexis to the tectonic evolution of Indian crust beneath southern Tibet: Geological Society of America Bulletin, v. 123, p. 218–239, doi:10.1130/B30085.1.

Kumar, G., 1997, Geology of Arunachal Pradesh: Bangalore, Geological Society of India, 217 p.

Lacassin, R., Valli, F., Arnaud, N., Leloup, P.H., Paquette, J.L., Li, H.B., Tapponnier, P., Chevalier, M.L., Guillot, S., Maheo, G.M., and Xu, Z.Q., 2004, Large-scale geometry, offset and kinematic evolution of the Karakorum fault, Tibet: Earth and Planetary Science Letters, v. 219, p. 255–269, doi:10.1016/S0012-821X(04)00006-8.

Lee, H.Y., Chung, S.L., Wang, Y.B., Zhu, D.C., Yang, J.H., Song, B., Liu, D.Y., and Wu, F.Y., 2007, Age, petrogenesis and geological significance of the Linizong volcanic successions in the Linzhou basin, southern Tibet: Evidence from zircon U-Pb dates and Hf isotopes: Acta Petrolei Sinica, v. 23, p. 493–500.

Lee, H.Y., Chung, S.L., Lo, C.H., Ji, J.Q., Lee, T.Y., Qian, Q., and Zhang, Q., 2009, Eocene Neotethyan slab breakoff in southern Tibet inferred from the Linzizong volcanic record: Tectonophysics, v. 477, p. 20–35, doi:10.1016/j.tecto.2009.02.031.

Leeder, M.R., Smith, A.B., and Yin, J., 1988, Sedimentology, palaeoecology and palaeoenvironmental evolution

of the 1985 Lhasa to Golmud Geotraverse: Royal Society of London Philosophical Transaction, ser. A, v. 327, p. 107–143, doi:10.1098/rsta.1988.0123.

LeFort, P., 1975, Himalayas: The collided range. Present knowledge of the continental arc: American Journal of Science, v. 275-A, p. 1–44.

LeFort, P., and Räi, S.M., 1999, Pre-Tertiary felsic magmatism of the Nepal Himalaya: Recycling of continental crust: Journal of Asian Earth Sciences, v. 17, p. 607–628, doi:10.1016/S1367-9120(99)00015-2.

Leier, A.L., Kapp, P., Gehrels, G.E., and DeCelles, P.G., 2007, Detrital zircon geochronology of Carboniferous–Cretaceous strata in the Lhasa terrane, southern Tibet: Basin Research, v. 19, p. 361–378, doi:10.1111/j.1365-2117.2007.00330.x.

Le Pera, E., and Arribas, J., 2004, Sand composition in an Iberian passive-margin fluvial course: The Tajo River: Sedimentary Geology, v. 171, p. 261–281, doi:10.1016/j.sedgeo.2004.05.019.

Le Pera, E., Arribas, J., Critelli, S., and Tortosa, A., 2001, The effects of source rocks and chemical weathering on the petrogenesis of siliciclastic sand from the Neto River (Calabria, Italy): Implications for provenance studies: Sedimentology, v. 48, p. 357–378, doi:10.1046/j.1365-3091.2001.00368.x.

Li, G.W., Liu, X.H., Pullen, A., Wei, L.J., Liu, X.B., Huang, F.X., and Zhou, X.J., 2010, In-situ detrital zircon geochronology and Hf isotopic analyses from Upper Triassic Tethys sequence strata: Earth and Planetary Science Letters, v. 297, p. 461–470, doi:10.1016/j.epsl.2010.06.050.

Liang, Y.H., Chung, S.L., Liu, D.Y., Xu, Y.G., Wu, F.Y., Yang, J.H., Wang, Y.B., and Lo, C.H., 2008, Detrital zircon evidence from Burma for reorganization of the eastern Himalayan river system: American Journal of Science, v. 308, p. 618–638, doi:10.2475/04.2008.08.

McQuarrie, N., Robinson, D., Long, S., Tobgay, T., Grujic, G., Gehrels, G., and Ducea, M., 2008, Preliminary stratigraphic and structural architecture of Bhutan: Implications for the along strike architecture of the Himalayan system: Earth and Planetary Science Letters, v. 272, p. 105–117, doi:10.1016/j.epsl.2008.04.030.

Medlicott, H.B., 1868, The Alps and the Himalayas, a geological comparison: Quarterly Journal of the Geological Society of London, v. 24, p. 34–52, doi:10.1144/GSL.JGS.1868.024.01-02.15.

Miller, C., Schuster, R., Klötzli, U., Frank, W., and Purtscheller, F., 1999, Post-collisional potassic and ultrapotassic magmatism in SW Tibet: Geochemical and Sr-Nd-Pb-O isotopic constraints for mantle source characteristics and petrogenesis: Journal of Petrology, v. 40, p. 1399–1424, doi:10.1093/petrology/40.9.1399.

Mo, X.X., Hou, Z.Q., Niu, Y.L., Dong, G.C., Qu, X.M., Zhao, Z.D., and Yang, Z.M., 2007, Mantle contributions to crustal thickening during continental collision: Evidence from Cenozoic igneous rocks in southern Tibet: Lithos, v. 96, p. 225–242, doi:10.1016/j.lithos.2006.10.005.

Mo, X.X., Dong, G.C., Zhao, Z.D., Zhu, D.C., and Zhou, S., 2009, Mantle input to the crust in southern Gangdese, Tibet, during the Cenozoic: Zircon Hf isotopic evidence: Journal of Earth Science, v. 20, p. 241–249, doi:10.1007/s12583-009-0023-2.

Montgomery, D.R., and Stolar, D.B., 2006, Reconsidering Himalayan river anticlines: Geomorphology, v. 82, p. 4–15, doi:10.1016/j.geomorph.2005.08.021.

Montgomery, D.R., Hallet, B., Liu, Y.P., Finnegan, N., Anders, A., Gillespie, A., and Greenberg, H.M., 2004, Evidence for Holocene megafloods down the Tsangpo River gorge, southeastern Tibet: Quaternary Research, v. 62, p. 201–207, doi:10.1016/j.yqres.2004.06.008.

Murphy, M.A., Yin, A., Harrison, T.M., Dürr, S.B., Chen, Z., Ryerson, F.J., Kidd, W.S.F., Wang, X., and Zhou, X., 1997, Did the Indo-Asian collision alone create the Tibetan Plateau: Geology, v. 25, p. 719–722, doi:10.1130/0091-7613(1997)025<0719:DTIACA>2.3.CO;2.

Myrow, P.M., Hughes, N.C., Paulsen, T.S., Williams, I.S., Parcha, S.D., Thompson, K.R., Bowering, S.A., Peng, S.C., and Ahluwalia, A.D., 2003, Integrated tectonostratigraphic analysis of the Himalaya and implications for its tectonic reconstruction: Earth and Planetary Science Letters, v. 212, p. 433–441, doi:10.1016/S0012-821X(03)00280-2.

Myrow, P.M., Hughes, N.C., Searle, M.P., Fanning, C.M., Peng, S.C., and Parcha, S.K., 2009, Stratigraphic correlation of Cambrian–Ordovician deposits along the Himalaya: Implications for the age and nature of rocks in the Mount Everest region: Geological Society of America Bulletin, v. 121, p. 323–332, doi:10.1130/B26384.1.

Myrow, P.M., Hughes, N.C., Goodge, J.W., Fanning, C.M., Williams, I.S., Peng, S.C., Bhargava, O.N., Parcha, S.K., and Pogue, K.B., 2010, Extraordinary transport and mixing of sediment across Himalayan central Gondwana during the Cambrian–Ordovician: Geological Society of America Bulletin, v. 122, p. 1660–1670, doi:10.1130/B30123.1.

Owen, L.A., Finkel, R.C., Ma, H., and Barnard, P.L., 2006, Late Quaternary landscape evolution in the Kunlun Mountains and Qaidam Basin, Northern Tibet: A framework for examining the links between glaciation, lake level changes and alluvial fan formation: Quaternary International, v. 154–155, p. 73–86, doi:10.1016/j.quaint.2006.02.008.

Pan, G.T., Ding, J., Yao, D.S., and Wang, L.Q., 2004, Geological Map of Qinghai-Xiang (Tibet) Plateau and Adjacent Areas: Chengdu, Chengdu Institute of Geology and Mineral Resources, China Geological Survey, scale 1:1,500,000, 6 sheets.

Pullen, A., Kapp, P., McCallister, A.T., Chang, H., Gehrels, G.E., Garzione, C.N., Heermance, R.V., and Ding, L., 2011, Qaidam basin and northern Tibetan Plateau as dust sources for the Chinese Loess Plateau and paleoclimatic implications: Geology, v. 39, p. 1031–1034, doi:10.1130/G32296.1.

Robl, J., Stüwe, K., and Hergarten, S., 2008, Channel profiles around Himalayan river anticlines: Constraints on their formation from digital elevation model analysis: Tectonics, v. 27, p. TC3010, doi:10.1029/2007TC002215.

Ryan, W.B.F., Carbotte, S.M., Coplan, J.O., O'Hara, S., Melkonian, A., Arko, R., Weissel, R.A., Ferrini, V., Goodwillie, A., Nitsche, F., Bonczkowski, J., and Zemsky, R., 2009, Global multi-resolution topography synthesis: Geochemistry, Geophysics, Geosystems, v. 10, p. Q03014, doi:10.1029/2008GC002332.

Seeber, L., and Gornitz, V., 1983, River profiles along the Himalayan arc as indicators of active tectonics: Tectonophysics, v. 92, p. 335–367, doi:10.1016/0040-1951(83)90201-9.

Stewart, R.J., Halley, B., Zeitler, P.K., Malloy, M.A., Allen, C.M., and Trippett, D., 2008, Brahmaputra sediment flux dominated by highly localized rapid erosion from the easternmost Himalaya: Geology, v. 36, p. 711–714, doi:10.1130/G24890A.1.

Sun, C.G., Zhao, Z.D., Mo, X.X., Zhu, D.C., Dong, G.C., Zhou, S., Chen, H.H., Xie, L.W., Yang, Y.H., Sun, J.F., and Yu, F., 2008, Enriched mantle source and petrogenesis of Sailipu ultrapotassic rocks in southwestern Tibetan Plateau: Constraints from zircon U-Pb geochronology and Hf isotopic compositions: Acta Petrolei Sinica, v. 24, p. 249–264.

Tapponnier, P., Peltzer, G., and Armijo, R., 1986, On the mechanics of the collision between India and Asia, *in* Coward, M.P., and Ries, A.C., eds., Collision Tectonics: Geological Society of London Special Publications 19, p. 113–157.

Thiede, R.C., Arrowsmith, R.J., Bookhagen, B., McWilliams, M.O., Sobel, E.R., and Strecker, M.R., 2005, From tectonically to erosionally controlled development of the Himalayan orogen: Geology, v. 33, p. 689–692, doi:10.1130/G21483.1.

Tobgay, T., Long, S., McQuarrie, N., Ducea, M.N., and Gehrels, G., 2010, Using isotopic and chronologic data to fingerprint strata: Challenges and benefits of variable sources to tectonic interpretations, the Paro Formation, Bhutan Himalaya: Tectonics, v. 29, p. TC6023, doi:10.1029/2009TC002637.

Wager, L.R., 1937, The Arun River drainage pattern and the rise of the Himalaya: The Geographical Journal, v. 89, p. 239–250, doi:10.2307/1785796.

Webb, A.A.G., Yin, A., Harrison, T.M., Célérier, J., Gehrels, G.E., Grove, M., Manning, C.E., and Burgess, W.P., 2011, Cenozoic tectonic history of the Himachal Himalaya (northwestern India) and its constraints on the formation mechanism of the Himalayan orogen: Geosphere, v. 7, p. 1013–1061, doi:10.1130/GES00627.1.

Wen, D.R., Liu, D.Y., Chung, S.L., Chu, M.F., Ji, J.Q., Zhang, Q., Song, B., Lee, T.Y., Yeh, M.W., and Lo, C.H., 2008, Zircon SHRIMP U-Pb ages of the Gangdese batholith and implications for Neotethyan subduction in southern Tibet: Chemical Geology, v. 252, p. 191–201, doi:10.1016/j.chemgeo.2008.03.003.

Williams, H., Turner, S., Kelley, S., and Harris, N., 2001, Age and composition of dikes in southern Tibet: New constraints on timing of east-west extension and its relationship to post-collisional volcanism: Geology, v. 29, p. 339–342, doi:10.1130/0091-7613(2001)029<0339:AACODI>2.0.CO;2.

Wu, F.Y., Yang, Y.H., Xie, L.W., Yang, J.H., and Xu, P., 2006, Hf isotopic compositions of the standard zircons and baddeleyites used in U-Pb geochronology: Chemical Geology, v. 234, p. 105–126, doi:10.1016/j.chemgeo.2006.05.003.

Wu, F.Y., Clift, P.D., and Yang, J.H., 2007, Zircon Hf isotopic constraints on the sources of the Indus molasse, Ladakh Himalaya, India: Tectonics, v. 26, p. TC2014, doi:10.1029/2006TC002051.

Wu, F.Y., Ji, W.Q., Liu, C.Z., and Chung, S.L., 2010, Detrital zircon U-Pb and Hf isotopic data from the Xigaze forearc basin: Constraints on Transhimalayan magmatic evolution in southern Tibet: Chemical Geology, v. 271, p. 13–25, doi:10.1016/j.chemgeo.2009.12.007.

Xie, L.W., Zhang, Y.B., Zhang, H.H., Sun, J.F., and Wu, F.Y., 2008, In situ simultaneous determination of trace elements, U-Pb and Lu-Hf isotopes in zircon and baddeleyite: Chinese Science Bulletin, v. 53, p. 1565–1573, doi:10.1007/s11434-008-0086-y.

Xu, R.H., Schärer, U., and Allègre, C.J., 1985, Magmatism and metamorphism in the Lhasa block (Tibet): A geochronological study: The Journal of Geology, v. 93, p. 41–57, doi:10.1086/628918.

Yin, A., 2006, Cenozoic tectonic evolution of the Himalayan orogen as constrained by along-strike variation of structural geometry, exhumation history, and foreland sedimentation: Earth-Science Reviews, v. 79, p. 163–164, doi:10.1016/j.earscirev.2006.08.005.

Yin, A., and Harrison, T.M., 2000, Geologic evolution of the Himalayan-Tibetan orogen: Annual Review of Earth and Planetary Sciences, v. 28, p. 211–280, doi:10.1146/annurev.earth.28.1.211.

Yin, A., Harrison, T.M., Ryerson, F.J., Chen, W.J., Kidd, W.S.F., and Copeland, P., 1994, Tertiary structural evolution of the Gangdese thrust system, southeastern Tibet: Journal of Geophysical Research–Solid Earth, v. 99, p. 18,175–18,201, doi:10.1029/94JB00504.

Yin, A., Harrison, T.M., Murphy, M.A., Grove, M., Nie, S., Ryerson, F.J., Wang, X.F., and Chen, Z.L., 1999, Tertiary deformation history of southeastern and southwestern Tibet during the Indo-Asian collision: Geological Society of America Bulletin, v. 111, p. 1644–1664, doi:10.1130/0016-7606(1999)111<1644:TDHOSA>2.3.CO;2.

Yin, A., Dubey, C.S., Kelty, T.K., Gehrels, G.E., Chou, C.Y., Grove, M., and Lovera, O.M., 2006, Structural evolution of the Arunachal Himalaya and implications for asymmetric development of the Himalayan orogen: Current Science, v. 90, p. 195–206.

Yin, A., Dubey, C.S., Webb, A.A.G., Kelty, T.K., Grove, M., Gehrels, G.E., and Burgess, W.P., 2010a, Geological correlation of the Himalayan orogen and Indian craton: Part 1. Structural geology, U-Pb zircon geochronology, and tectonic evolution of the Shillong Plateau and its neighboring regions in NE India: Geological Society of America Bulletin, v. 122, p. 336–359, doi:10.1130/B26460.1.

Yin, A., Dubey, C.S., Kelty, T.K., Webb, A.A.G., Harrison, T.M., Chou, C.Y., and Célérier, J., 2010b, Geological correlation of the Himalayan orogen and Indian craton: Part 2. Structural geology, geochronology, and tectonic evolution of the eastern Himalaya: Geological Society of America Bulletin, v. 122, p. 360–395, doi:10.1130/B26461.1.

Zeitler, P.K., Koons, P.O., Bishop, M.P., Chamberlain, C.P., Craw, D., Edwards, M.A., Hamidullah, S., Jan, M.Q., Khan, M.A., Khattak, M.U.K., Kidd, W.S.F., Mackie, R.L., Meltzer, A.S., Park, S.K., Pecher, A., Poage, M.A., Sarker, G., Schneider, D.A., Seeber, L., and Shroder, J.F., 2001, Crustal reworking at Nanga Parbat,

Pakistan: Metamorphic consequences of thermal-mechanical coupling facilitated by erosion: Tectonics, v. 20, p. 712–728, doi:10.1029/2000TC001243.

Zeng, L.S., Gao, L.E., Xie, K.J., and Liu, J., 2011, Mid-Eocene high Sr/Y granites in the northern Himalayan gneiss domes: Melting thickened lower continental crust: Earth and Planetary Science Letters, v. 303, p. 251–266, doi:10.1016/j.epsl.2011.01.005.

Zhang, D.D., 1998, Geomorphological problems of the middle reaches of the Tsangpo River, Tibet: Earth Surface Processes and Landforms, v. 23, p. 889–903, doi:10.1002/(SICI)1096-9837(199810)23:10<889::AID-ESP907>3.0.CO;2-E.

Zhang, D.D., 2001, Tectonically controlled fluvial landforms on the Yaluzangbu River and their implications for the evolution of the river: Mountain Research and Development, v. 21, p. 61–68, doi:10.1659/0276-4741(2001)021[0061:TCFLOT]2.0.CO;2.

Zhu, D.C., Pan, G.T., Mo, X.X., Wang, L.Q., Liao, Z.L., Jiang, X.S., and Geng, Q.R., 2005, SHRIMP U-Pb zircon dating for the dacite of the Sangxiu Formation in the central segment of Tethyan Himalaya and its implications: Chinese Science Bulletin, v. 50, p. 6563–6568.

Zhu, D.C., Pan, G.T., Mo, X.X., Liao, Z.L., Jiang, X.S., Wang, L.Q., and Zhao, Z.D., 2007, Petrogenesis of volcanic rocks in the Sangxiu Formation, central segment of Tethyan Himalaya: A probable example of plume-lithosphere interaction: Journal of Asian Earth

Sciences, v. 29, p. 320–335, doi:10.1016/j.jseaes.2005.12.004.

Zhu, D.C., Mo, X.X., Pan, G.T., Zhao, Z.D., Dong, G.C., Shi, Y.R., Liao, Z.L., Wang, L.Q., and Zhou, C.Y., 2008a, Petrogenesis of the earliest Early Cretaceous mafic rocks from the Cona area of the eastern Tethyan Himalayan in south Tibet: Interaction between the incubating Kerguelen plume and the eastern Greater India lithosphere: Lithos, v. 100, p. 147–173, doi:10.1016/j.lithos.2007.06.024.

Zhu, D.C., Mo, X.X., Zhao, Z.D., Niu, Y.L., and Chung, S.L., 2008b, Whole-rock elemental and zircon Hf isotopic geochemistry of mafic and ultramafic rocks from the Early Cretaceous Comei large igneous province in SE Tibet: Constraints on mantle source characteristics and petrogenesis: Himalayan Journal of Sciences, v. 5, p. 178–180, doi:10.3126/hjs.v5i7.1350.

Zhu, D.C., Pan, G.T., Chung, S.L., Liao, Z.L., Wang, L.Q., and Li, G.M., 2008c, SHRIMP zircon age and geochemical constraints on the origin of Lower Jurassic volcanic rocks from the Yeba Formation, southern Gangdese, southern Tibet: International Geology Review, v. 50, p. 442–471, doi:10.2747/0020-6814.50.5.442.

Zhu, D.C., Chung, S.L., Mo, X.X., Zhao, Z.D., Niu, Y.L., Song, B., and Yang, Y.H., 2009a, The 132 Ma Comei-Bunbury large igneous province: Remnants identified in present-day southeastern Tibet and southwestern Australia: Geology, v. 37, p. 583–586, doi:10.1130/G30001A.1.

Zhu, D.C., Mo, X.X., Niu, Y.L., Zhao, Z.D., Wang, L.Q., Liu, Y.S., and Wu, F.Y., 2009b, Geochemical investigation of Early Cretaceous igneous rocks along an east-west traverse throughout the central Lhasa terrane, Tibet: Chemical Geology, v. 268, p. 298–312, doi:10.1016/j.chemgeo.2009.09.008.

Zhu, D.C., Zhao, Z.D., Pan, G.T., Lee, H.Y., Kang, Z.Q., Liao, Z.L., Wang, L.Q., Li, G.M., Dong, G.C., and Liu, B., 2009c, Early Cretaceous subduction-related adakite-like rocks of the Gangdese belt, southern Tibet: Products of slab melting and subsequent melt-peridotite interaction?: Journal of Asian Earth Sciences, v. 34, p. 298–309, doi:10.1016/j.jseaes.2008.05.003.

Zhu, D.C., Zhao, Z.D., Niu, Y.L., Mo, X.X., Chung, S.L., Hou, Z.Q., Wang, L.Q., and Wu, F.Y., 2011, The Lhasa terrane: Record of a microcontinent and its histories of drift and growth: Earth and Planetary Science Letters, v. 301, p. 241–255, doi:10.1016/j.epsl.2010.11.005.